Inorg. Chem. **2005**, *44*, 8770–8785

Syntheses; ^{77}Se, ^{203}Tl, and ^{205}Tl NMR; and Theoretical Studies of the $Tl_2Se_6^{6-}$, $Tl_3Se_6^{5-}$, and $Tl_3Se_7^{5-}$ Anions and the X-ray Crystal Structures of [2,2,2-crypt-Na]$_4$[Tl_4Se_8]·en and [2,2,2-crypt-Na]$_2$[Tl_2Se_4]$^1_\infty$·en

Ayaaz M. Pirani,[†] Hélène P. A. Mercier,*[,†] Reijo J. Suontamo,[‡] Gary J. Schrobilgen,*[,†] David P. Santry,[†] and Horst Borrmann[§]

Department of Chemistry, McMaster University, Hamilton, Ontario L8S 4M1, Canada, Department of Chemistry, University of Jyväskylä, P.O. Box 35, FIN-40014, Finland, and Max-Planck-Institut für Chemische Physik fester Stoffe, Raum B1.2.11, Nöthnitzer Strasse 40, Dresden D-01187, Germany

Received June 30, 2005

The 2,2,2-crypt salts of the $Tl_4Se_8^{4-}$ and $[Tl_2Se_4^{2-}]^1_\infty$ anions have been obtained by extraction of the ternary alloy $NaTl_{0.5}Se$ in ethylenediamine (en) in the presence of 2,2,2-crypt and 18-crown-6 followed by vapor-phase diffusion of THF into the en extract. The [2,2,2-crypt-Na]$_4$[Tl_4Se_8]·en crystallizes in the monoclinic space group $P2_1/n$, with $Z = 2$ and $a = 14.768(3)$ Å, $b = 16.635(3)$ Å, $c = 21.254(4)$ Å, $\beta = 94.17(3)°$ at –123 °C, and the [2,2,2-crypt-Na]$_2$[Tl_2Se_4]$^1_\infty$·en crystallizes in the monoclinic space group $P2_1/c$, with $Z = 4$ and $a = 14.246(2)$ Å, $b = 14.360(3)$ Å, $c = 26.673(8)$ Å, $\beta = 99.87(3)°$ at –123 °C. The Tl^{III} anions, $Tl_2Se_6^{6-}$ and $Tl_3Se_7^{5-}$, and the mixed oxidation state Tl^I/Tl^{III} anion, $Tl_3Se_6^{5-}$, have been obtained by extraction of $NaTl_{0.5}Se$ and NaTlSe in en, in the presence of 2,2,2-crypt and/or in liquid NH_3, and have been characterized in solution by low-temperature ^{77}Se, ^{203}Tl, and ^{205}Tl NMR spectroscopy. The $^1J(^{203,205}Tl–^{77}Se)$ and $^2J(^{203,205}Tl–^{203,205}Tl)$ couplings of the three anions have been used to arrive at their solution structures by detailed analyses and simulations of all spin multiplets that comprise the ^{205,203}Tl NMR subspectra arising from natural abundance ^{205,203}Tl and ^{77}Se isotopomer distributions. The structure of $Tl_2Se_6^{6-}$ is based on a Tl_2Se_2 ring in which each thallium is bonded to two exo-selenium atoms so that these thalliums are four-coordinate and possess a formal oxidation state of +3. The $Tl_4Se_8^{4-}$ anion is formally derived from the $Tl_2Se_6^{6-}$ anion by coordination of each pair of terminal Se atoms to the Tl^{III} atom of a $TlSe^+$ cation. The structure of the $[Tl_2Se_4^{2-}]^1_\infty$ anion is comprised of edge-sharing distorted $TlSe_4$ tetrahedra that form infinite, one-dimensional $[Tl_2Se_4^{2-}]^1_\infty$ chains. The structures of $Tl_3Se_6^{5-}$ and $Tl_3Se_7^{5-}$ are derived from Tl_4Se_4-cubes in which one thallium atom has been removed and two and three exo-selenium atoms are bonded to thallium atoms, respectively, so that each is four-coordinate and possesses a formal oxidation state of +3 with the remaining three-coordinate thallium atom in the +1 oxidation state. Quantum mechanical calculations at the MP2 level of theory show that the $Tl_2Se_6^{6-}$, $Tl_3Se_6^{5-}$, $Tl_3Se_7^{5-}$, and $Tl_4Se_8^{4-}$ anions exhibit true minima and display geometries that are in agreement with their experimental structures. Natural bond orbital and electron localization function analyses were utilized in describing the bonding in the present and previously published Tl/Se anions, and showed that the $Tl_2Se_6^{6-}$, $Tl_3Se_6^{5-}$, $Tl_3Se_7^{5-}$, and $Tl_4Se_8^{4-}$ anions are electron-precise rings and cages.

Introduction

The number of thallium chalcogenide anions is small in comparison to the chalcogenide anions of other group 13 elements as summarized in ref 1 which should be consulted for an overview of the subject. In that paper we reported a new series of thallium selenide polyanions, i.e., $Tl_4Se_5^{4-}$, $Tl_4Se_6^{4-}$, and $Tl_5Se_5^{3-}$, which were obtained by extraction of KTlSe in ethylenediamine (en) or liquid NH_3 in the presence of 2,2,2-crypt. While the $Tl_2Se_2^{2-}$ [2] and $Tl_5Se_5^{3-}$ [1]

* To whom correspondence should be addressed. E-mail: schrobil@mcmaster.ca (G.J.S.).
[†] McMaster University.
[‡] University of Jyväskylä.
[§] Max-Planck-Institut.

(1) Campbell, J.; Mercier, H. P. A.; Santry, D. P.; Suontamo, R. J.; Borrmann, H.; Schrobilgen, G. J. *Inorg. Chem.* **2001**, *40*, 233.

10.1021/ic0510922 CCC: $30.25
Published on Web 10/28/2005

Table 1. Summary of Crystal Data and Refinement Results for [2,2,2-crypt-Na]$_4$[Tl_4Se_8]·en and [2,2,2-crypt-Na]$_2$[Tl_2Se_4]$^1_\infty$·en[a]

	[2,2,2-crypt-Na]$_4$[Tl_4Se_8]·en	[2,2,2-crypt-Na]$_2$[Tl_2Se_4]$^1_\infty$·en
formula	$C_{74}H_{152}N_{10}O_{24}$ $Na_4Tl_4Se_8$	$C_{38}H_{80}O_{12}N_6Na_2Se_4Tl_2$
mol. wt.	3107.18	1583.64
space group (no.)	$P2_1/n$ (15)	$P2_1/c$ (15)
a, Å	14.768(3)	14.246(2)
b, Å	16.635(3)	14.360(3)
c, Å	21.254(4)	26.673(8)
β, deg	94.17(3)	99.87(3)
V, Å^{-3}	5207.6(18)	5375.8(25)
Z	2	4
T, °C	−123	−123
ρ_{calc}, g cm^{-3}	1.982	1.957[b]
μ, cm^{-1}	9.051	8.77
R_1, $F^2 > 2\sigma F^2$	0.0331	0.0447
wR_2, F^2	0.0446	0.1133

[a] $R_1 = \sum||F_o| - |F_c||/\sum|F_o|$ for $I > 2\sigma(I)$. [b] $wR_2 = [\sum[w(F_o^2 - F_c^2)^2]/\sum w(F_o^2)^2]^{1/2}$ for $I > 2\sigma(I)$. [b] The experimental density is >1.92 as determined by flotation in perfluorodecaline.

anions could be characterized by single-crystal X-ray structure determination, the $TlSe_3^{3-}$,[2,3] $Tl_2Se_2^{2-}$,[2,3] $Tl_4Se_5^{4-}$,[1] and $Tl_4Se_6^{4-}$ [1] anions were characterized in solution by ^{203,205}Tl and ^{77}Se NMR spectroscopy. The $Tl_4Se_5^{4-}$, $Tl_4Se_6^{4-}$, and $Tl_5Se_5^{3-}$ anions are the first mixed oxidation state Tl^I/Tl^{III} and cubanoid tetrathallium selenide cages to have been reported, and represent rare examples of group 13 chalcogenide cages, among which are $Ga_4S_{10}^{8-}$,[4] $Ga_4Se_{10}^{8-}$,[5] $In_4S_{10}^{8-}$,[4] $In_4Se_{10}^{8-}$,[4] and $In_3Te_7^{5-}$.[6]

This paper represents a significant extension of thallium selenide chemistry, reporting the detailed variable-temperature solution multi-NMR spectroscopic characterization of the Tl^{III} anions, $Tl_2Se_6^{6-}$ and $Tl_3Se_7^{5-}$, the mixed oxidation state Tl^I/Tl^{III} anion, $Tl_3Se_6^{5-}$, and the X-ray crystal structures of the Tl^I/Tl^{III} anion, $Tl_4Se_8^{4-}$, and the Tl^{III} anion, $[Tl_2Se_4^{2-}]^1_\infty$.

Results and Discussion

Syntheses of the Polythallium Selenide Anions. The title polyanions were synthesized from the ternary alloys NaTlSe and $NaTl_{0.5}Se$ by fusion of the elements followed by extraction of the powdered alloys in en and en/THF (1:1 v/v) in the presence of an excess of 2,2,2-crypt (4,7,13,16,21,24-hexaoxa-1,10-diazabicyclo-[8.8.8]hexacosane), with respect to Na^+. The extractions were also carried out in liquid NH_3 in the absence of 2,2,2-crypt.[7] The ^{203}Tl, ^{205}Tl, and ^{77}Se NMR spectra indicated that solutions prepared by extraction of NaTlSe and $NaTl_{0.5}Se$ contained the same polyanions; however, extracts of the latter alloy with no 2,2,2-crypt added generally contained higher concentrations of the polyanions of interest and gave rise to sharper and better-resolved NMR spectra. Consequently, the ensuing discussion of the NMR parameters refers to spectra recorded for the $NaTl_{0.5}Se$ extracts in liquid NH_3 at −70 °C (see NMR Spectroscopy).

Attempts to obtain suitable single crystals by the vapor-phase diffusion of THF into en extracts of NaTlSe or $NaTl_{0.5}Se$ containing a molar excess or deficit of 2,2,2-crypt with respect to Na^+ failed to yield crystalline material over an 8−12 month period. Crystals suitable for X-ray structure determinations were, however, obtained over a period of 8 months by vapor-phase diffusion of THF into en extracts of $NaTl_{0.5}Se$ containing an equimolar mixture of 18-crown-6 and 2,2,2-crypt, where the total amount of 2,2,2-crypt and 18-crown-6 was in stoichiometric excess of the available Na^+ ion.

X-ray Crystal Structures of [2,2,2-crypt-Na]$_4$[Tl_4Se_8]·en and [2,2,2-crypt-Na]$_2$[Tl_2Se_4]$^1_\infty$·en. A summary of the crystal data and refinement results is given in Table 1. The most significant bond lengths, bond angles, and long contact distances are given in Table 2. The structures of the 2,2,2-crypt-Na^+ cations are similar to those previously reported in [2,2,2-crypt-Na]$_2$[Te_4][8] and [2,2,2-crypt-Na]$_2$[$Cr_2(CO)_{10}$][9] with Na···N distances of 2.77(3)−3.06(2) and 2.716(2)−3.162(2) Å, respectively. The solvent molecules in the [$Tl_2Se_4^{2-}$] salt are positionally disordered with 60:40 site occupancies corresponding to two en molecule orientations.

(a) [2,2,2-crypt-Na]$_4$[Tl_4Se_8]·en. The most interesting aspect of the structure is the geometry of the $Tl_4Se_8^{4-}$ anion ($\sim C_{2v}$ point symmetry) in which the thallium atoms are formally in the +3 oxidation state, but are in two chemical environments: two thallium atoms display trigonal planar coordination [Tl_P] to three selenium atoms and the remaining two thallium atoms are tetrahedrally coordinated [Tl_T] to four selenium atoms (Figure 1a). The selenium atoms are in three chemical environments: terminal Se_t atoms, Se_b atoms bridging Tl_P and Tl_T atoms, and $Se_{b'}$ atoms bridging Tl_T atoms. Accordingly, four distinct Tl−Se bond distances are observed which increase in the order Tl_P−Se_t [2.4653(8) Å] < Tl_P−Se_b [2.5965(9)−2.6167(9) Å] < Tl_T−$Se_{b'}$ [2.6341(9)

(2) Borrmann, H.; Campbell, J.; Dixon, D. A.; Mercier, H. P. A.; Pirani, A. M.; Schrobilgen, G. J. *Inorg. Chem.* **1998**, *37*, 1929.
(3) Burns, R. C.; Devereux, L. A.; Granger, P.; Schrobilgen, G. J. *Inorg. Chem.* **1985**, *24*, 2615.
(4) Krebs, B.; Voelker, D.; Stiller, K. O. *Inorg. Chim. Acta* **1982**, *65*, L101.
(5) Deiseroth, H. J. *Z. Kristallogr.* **1984**, *166*, 283.
(6) Park, C.-W.; Salm, R. J.; Ibers, J. A. *Angew. Chem., Int. Ed. Engl.* **1995**, *34*, 1879.
(7) The extractions were also carried out in liquid NH_3 in the presence of molar excesses or deficits of 2,2,2-crypt or 18-crown-6, but gave rise to large amounts of colorless crystalline material at temperatures below −20 °C.
(8) Devereux, L. A.; Schrobilgen, G. J.; Sawyer, J. F. *Acta Crystallogr.* **1985**, *C41*, 1730.
(9) Borrmann, H.; Pirani, A. M.; Schrobilgen, G. J. *Acta Crystallogr.* **1997**, *C53*, 19.

Table 2. Experimental and Calculated Geometries for the $Tl_4Se_8^{4-}$ and $[Tl_2Se_4^{2-}]_\infty^1$ Anions (Distances in Angstroms, and Angles in Degrees)

		$Tl_4Se_8^{4-}$ in [2,2,2-crypt-Na]$_4$[Tl_4Se_8]·en[a]			
Tl(1)−Se(1)	2.4653(8)	Tl(1)−Se(2)	2.5965(9)	Tl(1)−Se(3)	2.6167(9)
Tl(2)−Se(2)	2.6748(9)	Tl(2)−Se(3)	2.6632(9)	Tl(2)−Se(4)	2.6341(9)
Tl(1)···Tl(2)	3.5538(6)				
Se(1)−Tl(1)−Se(2)	133.44(3)	Se(3)−Tl(1)−Se(2)	93.62(2)	Se(4)−Tl(1)−Se(3A)	117.75(2)
Se(3)−Tl(1)−Se(3)	96.58(2)	Tl(1)−Se(2)−Tl(3)	84.61(2)	Se(4)−Tl(1)−Se(2A)	115.91(3)
Se(4)−Tl(1)−Se(3)	118.71(3)	Se(1)−Tl(1)−Se(3)	129.90(3)	Tl(1)−Se(2)−Tl(2)	84.77(2)
Se(4)−Tl(1)−Se(2)	116.50(3)	Se(4)−Tl(1)−Se(4A)	96.10(3)	Tl(2)−Se(2)−Tl(2A)	83.90(3)

$Tl_4Se_8^{4-}$ at the MP2/Stutt RLC ECP (2d) Level[b]

	MP2 (C_i)	MP2 (D_{2h})		MP2 (C_i)	MP2 (D_{2h})
Tl(1)−Se(1)	2.556	2.556	Tl(1)−Se(2)	2.656	2.656
Tl(1)−Se(3)	2.656	2.656	Tl(2)−Se(2)	2.787	2.787
Tl(2)−Se(3)	2.788	2.787	Tl(2)−Se(4)	2.715	2.716
Tl(2)−Se(5)	2.715	2.716	Tl(3)−Se(4)	2.715	2.716
Tl(3)−Se(5)	2.715	2.716	Tl(3)−Se(6)	2.788	2.787
Tl(3)−Se(7)	2.787	2.787	Tl(4)−Se(6)	2.656	2.656
Tl(4)−Se(7)	2.656	2.656	Tl(4)−Se(8)	2.556	2.556
Tl(1)···Tl(2)	3.708	3.708	Tl(2)...Tl(3)	3.673	3.674
Tl(3)···Tl(4)	3.708	3.708			
Se(1)−Tl(1)-Se(2)	131.4	131.4	Se(1)−Tl(1)−Se(3)	131.4	131.4
Se(2)−Tl(1)−Se(3)	97.1	97.1	Se(2)−Tl(2)−Se(3)	91.2	91.2
Se(2)−Tl(2)−Se(4)	118.3	118.3	Se(3)−Tl(2)−Se(4)	118.3	118.3
Se(3)−Tl(2)−Se(5)	118.2	118.3	Se(2)−Tl(2)−Se(5)	118.2	118.3
Se(4)−Tl(2)−Se(5)	94.9	94.9	Tl(1)−Se(2)−Tl(2)	85.8	85.8
Tl(1)−Se(3)−Tl(2)	85.8	85.8	Tl(2)−Se(4)−Tl(3)	85.1	85.1
Se(6)−Tl(4)−Se(8)	131.4	131.4	Se(7)−Tl(4)−Se(8)	131.4	131.4
Se(6)−Tl(4)−Se(7)	97.1	97.1	Se(4)−Tl(3)−Se(6)	118.2	118.3
Se(4)−Tl(3)−Se(7)	118.2	118.3	Se(4)−Tl(3)−Se(5)	94.9	94.9
Se(6)−Tl(3)−Se(7)	91.2	91.2	Se(6)−Tl(3)−Se(5)	118.3	118.3
Se(7)−Tl(3)−Se(5)	118.3	118.3	Tl(4)−Se(6)−Tl(3)	85.8	85.8
Tl(4)−Se(7)−Tl(3)	85.8	85.8	Tl(2)−Se(5)−Tl(3)	85.1	85.1

		$Tl_2Se_4^{2-}$ in [2,2,2-crypt-Na]$_2$[Tl_2Se_4]$_\infty^1$·en[a]			
Tl(1)−Se(1)	2.6513(10)	Tl(1)−Se(2)	2.6766(10)	Tl(1)−Se(3)	2.6520(9)
Tl(1)−Se(4)	2.6638(9)	Tl(2)−Se(1A)	2.6693(10)	Tl(2)−Se(2A)	2.6368(10)
Tl(2)−Se(3)	2.6513(9)	Tl(2)−Se(4)	2.6608(9)		
Tl(1)···Tl(2)	3.5983(8)				
Se(1)−Tl(1)−Se(3)	117.94(3)	Tl(2)−Se(4)−Tl(1)	85.03(3)	Se(4)−Tl(1)−Se(2)	117.76(3)
Se(3)−Tl(1)−Se(4)	94.59(3)	Tl(1)−Se(2)−Tl(2A)	85.02(3)	Se(3)−Tl(2)−Se(1B)	115.22(3)
Se(3)−Tl(1)−Se(2)	117.53(4)	Se(1)−Tl(1)−Se(4)	116.44(4)	Tl(2)−Se(3)−Tl(1)	85.45(3)
Se(3)−Tl(2)−Se(4)	94.67(3)	Se(1)−Tl(1)−Se(2)	94.48(3)	Tl(1)−Se(1)−Tl(2A)	84.88(3)
Se(4)−Tl(2)−Se(1B)	117.84(3)				

[a] The atom numbering scheme refers to that used in Figure 1. [b] The atom numbering scheme refers to that used in Figure 6c.

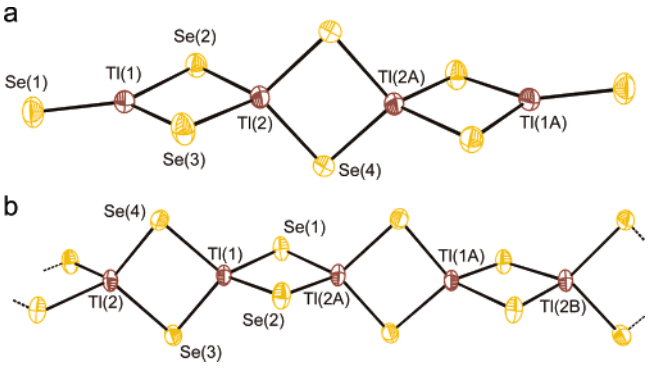

Figure 1. Views of (a) the $Tl_4Se_8^{4-}$ anion in [2,2,2-crypt-Na]$_4$[Tl_4Se_8]·en and (b) the $[Tl_2Se_4^{2-}]_\infty^1$ anion in [2,2,2-crypt-Na]$_2$[Tl_2Se_4]$_\infty^1$·en. Displacement ellipsoids are drawn at the 90% probability level.

Å] < Tl_T−Se_b [2.6632(9)−2.6748(9) Å]. The Tl−Se bond length correlation with thallium and selenium coordination numbers is consistent with the total bond valence concept.[10] The trend, Tl−Se_t < Tl−Se_b/Tl−$Se_{b'}$, is consistent with the calculated higher relative bond orders of the Tl−Se_t bonds (see Computational Results) and has been observed for terminal tin−chalcogen bonds in $Sn_2Ch_6^{4-}$,[11] $Sn_2Te_7^{4-}$,[12] and $Sn_4Ch_{10}^{4-}$ (Ch = Se[13] or Te[14]). Similar Tl_T−Se distances have been reported for the structures of $Tl_3Se_3(Se_4)_3^{3-}$ [2.64(3) Å],[15] $Tl_4Se_{16}^{4-}$ [2.66(3) Å],[16] $Tl(Se_6)_2^{2-}$ [2.639(2) Å],[17] and $Tl_5Se_5^{3-}$ [2.65(6) Å].[1] The Tl^{III}···Tl^{III} distance in $Tl_4Se_8^{4-}$ is 3.5538(6) Å and is considerably shorter than the average Tl^{III}···Tl^{III} distances observed in $Tl_3Se_3(Se_4)_3^{3-}$ [3.76(9) Å][15] and $Tl_4Se_{16}^{4-}$ [3.71(13) Å],[16] which is consistent with the two modes of coordination observed for the thallium atoms in the present anion structure (trigonal planar and tetrahedral) when compared with the single coordination

(10) O'Keeffe, M. *Struct. Bonding* **1989**, *71*, 162.
(11) Campbell, J.; Devereux, L. A.; Gerken, M.; Mercier, H. P. A.; Pirani, A. M.; Schrobilgen, G. J. *Inorg. Chem.* **1996**, *35*, 2945.
(12) Brinkmann, C.; Eisenmann, B.; Schäfer, H. *Mater. Res. Bull.* **1985**, *20*, 299.
(13) Campbell, J.; DiCiommo, D. P.; Mercier, H. P. A.; Pirani, A. M.; Schrobilgen, G. J.; Willuhn, M. *Inorg. Chem.* **1995**, *34*, 6265.
(14) Pirani, A. M.; Mercier, H. P. A.; Dixon, D. A.; Borrmann, H.; Schrobilgen, G. J. *Inorg. Chem.* **2001**, *40*, 4823.
(15) Dhingra, S.; Kanatzidis, M. G. *Inorg. Chem.* **1993**, *32*, 1350.
(16) Dhingra, S.; Liu, F.; Kanatzidis, M. G. *Inorg. Chim. Acta* **1993**, *210*, 237.
(17) Dhingra, S.; Kanatzidis, M. G. *Science* **1992**, *258*, 1769.

environment (tetrahedral) observed in the previously characterized anion structures.[1] The $Tl^{III}\cdots Tl^{III}$ bond distance was not reported for the $Tl(Se_6)_2^{2-}$ anion.[17]

The average $Se-Tl_T-Se$ bond angle in $Tl_4Se_8^{4-}$ [109.8(48)°] is close to the ideal tetrahedral angle and is similar to those observed in $Tl_3Se_3(Se_4)_3^{3-}$ [109.3(12)°],[15] $Tl_4Se_{16}^{4-}$ [108.8(22)°],[16] $Tl(Se_6)_2^{2-}$ [110.0(14)°],[17] and $Tl_5Se_5^{3-}$ [108.1(63)°][1] whereas the average $Se-Tl_P-Se$ bond angle, 119.9(12)°, is close to the ideal trigonal planar angle. The average Tl−Se−Tl bond angle [84.4(27)°] is similar to that in $Tl_5Se_5^{3-}$ [85.8(44)°][1] but is significantly less than those in $Tl_3Se_3(Se_4)_3^{3-}$ [93.9(16)°][15] and in $Tl_4Se_{16}^{4-}$ [89.2(93)°].[16] The Tl−Se−Tl and Se−Tl−Se bond angles for $Tl(Se_6)_2^{2-}$ are not available.[17]

(b) $[2,2,2\text{-crypt-Na}]_2[Tl_2Se_4]^1_\infty\cdot$en. The anion is comprised of edge-sharing, distorted $TlSe_4$ tetrahedra forming an infinite, one-dimensional chain running parallel to the *b*-axis of the unit cell (Figures 1b and S1) and is isostructural and isovalent with $In_2Te_4^{2-}$.[18] The anion chains are isolated from one another by 2,2,2-crypt-Na^+ cations and disordered en molecules and are noncommensurate with respect to the cations and solvent molecules. The $In_2Te_4^{2-}$ anion also occurs as an infinite chain within channels defined by the cations in the crystal structure of $[(n\text{-}C_4H_9)_4N]_2[In_2Te_4]$.[18] The only other infinite chain Tl/Se structure reported prior to this work is the alloy phase, TlSe.[19] In the latter case, the infinite chains are comprised of alternating Tl^{III} and Tl^{I} atoms which are not isolated from each other, but have additional contacts between adjacent chains. The $Tl^{III}-Se$ [2.6358(11)−2.6753(11) Å] and $Tl^{III}\cdots Tl^{III}$ [3.5985(9) Å] distances in the title compound are considerably shorter and longer, respectively, than those reported in TlSe [$Tl^{III}-Se$, 2.670(2) and $Tl^{III}\cdots Tl^{III}$, 3.486(1) Å], but are similar to the $Tl_T-Se_{b'}$ and Tl···Tl distances in $Tl_4Se_8^{4-}$ and in the previously reported Tl/Se anion structures (vide supra). The average Se−Tl−Se [109.6(38)°] bond angle is typical for Tl^{III} [1] and is similar to those of $Tl_4Se_8^{4-}$. The Tl−Se−Tl bond angle [85.1(12)°] is in good agreement with those of $Tl_4Se_8^{4-}$ and $Tl_5Se_5^{3-}$ (vide supra).

Solution Characterization of the $Tl_2Se_6^{6-}$, $Tl_3Se_6^{5-}$, and $Tl_3Se_7^{5-}$ Anions by NMR Spectroscopy. The $Tl_2Se_6^{6-}$, $Tl_3Se_6^{5-}$, and $Tl_3Se_7^{5-}$ anions were identified in en, en/THF (1:1 v/v), and/or liquid NH_3 solutions by direct observation of the spin-$^1/_2$ nuclides ^{205}Tl, ^{203}Tl, and ^{77}Se at their natural abundance levels. Key experimental and simulated ^{205}Tl, ^{203}Tl, and ^{77}Se NMR spectra are depicted in Figures 2−4, S2, and S3. The chemical shifts and spin−spin coupling constants, *J*, are summarized in Table 3 (NaTlSe) and Table 4 ($NaTl_{0.5}Se$). The number of observed environments, the multiplet patterns arising from $^2J(^{203(5)}Tl-^{205(3)}Tl)$ and $^1J(^{77}Se-^{205(3)}Tl)$, the satellite spacings corresponding to $^2J(^{205}Tl-^{203}Tl)$ and $^1J(^{205(3)}Tl-^{77}Se)$, and the satellite-to-central peak intensity ratios are consistent with the $Tl_2Se_6^{6-}$ (structure I), $Tl_3Se_6^{5-}$ (structure II), and $Tl_3Se_7^{5-}$ (structure III) anions having D_{2h}, C_{2v}, and C_{3v} point symmetries, respectively. The geometries deduced from NMR solution studies are supported by computational studies (see Computational Results).

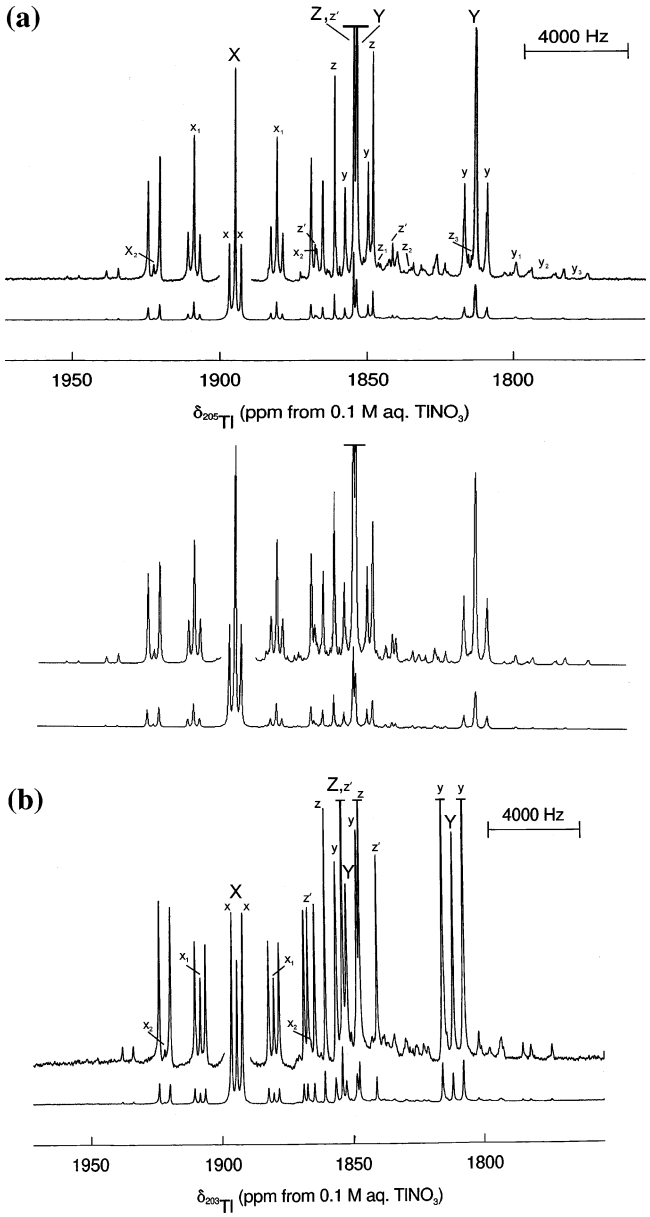

Figure 2. Thallium NMR spectra (liquid NH_3, −70 °C) of the Tl^{III} environment of (X) $Tl_2Se_6^{6-}$, (Y) $Tl_3Se_6^{5-}$, and (Z) $Tl_3Se_7^{5-}$ anions obtained by extraction of $NaTl_{0.5}Se$ into liquid NH_3: (a) experimental (upper trace) and calculated (lower trace) ^{205}Tl (115.444 MHz) and (b) experimental ^{203}Tl (114.319 MHz) spectra. For clarity, only the subspectra associated with the central lines of the multiplets are labeled. Peak labels are assigned as follows: $Tl_2Se_6^{6-}$ (X = S; x = $S/^2d_{Tl^{III}}^{Tl^{III}}$; x_1 = $S/^1d_{Se_b}^{Tl^{III}}$; x_2 = $S/^1d_{Se_t}^{Tl^{III}}$); $Tl_3Se_6^{5-}$ (Y = D; y = $D/^2d_{Tl^{III}}^{Tl^{III}}$; y_1 = $D/^1d_{Se_{b''}}^{Tl^{III}}$; y_2 = $D/^1d_{Se_{b'''}}^{Tl^{III}}$; y_3 = $D/^1d_{Se_t}^{Tl^{III}}$); $Tl_3Se_7^{5-}$ (Z = S; z = $S/^2d_{Tl^{III}}^{Tl^{III}}$; z′ = $S/^2t_{Tl^{III}}^{Tl^{III}}$; z_1 = $S/^1d_{Se_b}^{Tl^{III}}$; z_2 = $S/^1d_{Se_t}^{Tl^{III}}$). The multiplicity labels are defined in Table 5, footnote *c*.

In addition to the known $TlSe_3^{3-}$ anion (triplet, 2942 ppm), the ^{205}Tl and ^{203}Tl NMR spectra (−70 °C) of the red−orange liquid NH_3 extract of NaTlSe revealed four new resonances that were assigned to $Tl_2Se_6^{6-}$ (singlet, 1895 ppm), $Tl_3Se_6^{5-}$ (doublet, 1836 and triplet, 5284 ppm), and $Tl_3Se_7^{5-}$ (singlet, 1857 ppm). The corresponding resonances in the ^{77}Se spectrum (−74 °C) were assigned to $TlSe_3^{3-}$ (singlet, 78

(18) Warren, C. J.; Dhingra, S. S.; Haushalter, R. C.; Bocarsly, A. B. *J. Solid State Chem.* **1994**, *112*, 340.
(19) Ketelaar, J. A. A.; t'Hart, W. H.; Moerel, M.; Polder, D. *Z. Kristallogr.* **1939**, A101.

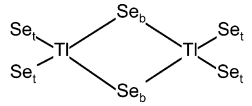

Structure I

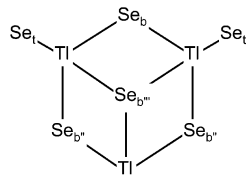

Structure II

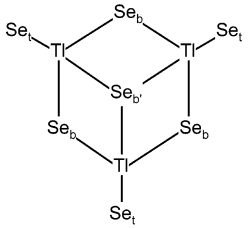

Structure III

ppm), $Tl_2Se_6^{6-}$ (very strong doublet, −101 and triplet, 209 ppm), and $Tl_3Se_6^{5-}$ (doublets, 63 and 32 ppm).

The ^{205}Tl NMR spectrum (0 °C) of the en extract of NaTlSe in the presence of 2,2,2-crypt revealed four signals that could be assigned to $Tl_3Se_6^{5-}$ (a doublet, 1825 ppm and a triplet, 5300 ppm), $Tl_4Se_6^{4-}$ (very broad triplet, 5180 ppm), and $TlSe_3^{3-}$ (triplet, 2875 ppm) (Figure S2). Only Se^{2-} (−432 ppm) and $TlSe_3^{3-}$ (134 ppm) were observed in the ^{77}Se spectrum (0 °C).

The ^{205}Tl and ^{203}Tl NMR spectra (−15 °C) of the orange en/THF extract of NaTlSe obtained in the presence of 2,2,2-crypt revealed two overlapping signals that were assigned to $Tl_2Se_6^{6-}$ (broadened singlet, 1877 ppm) and $Tl_3Se_6^{5-}$ (doublet, 1849 ppm) (Figure S3).

The ^{205}Tl and ^{203}Tl NMR spectra (−70 °C, Figures 2 and 3) of the deep-red NH_3 extract of $NaTl_{0.5}Se$ revealed the presence of $Tl_2Se_6^{6-}$ (singlet, 1895 ppm), $Tl_3Se_6^{5-}$ (doublet, 1833 ppm and triplet, 5276 ppm), and $Tl_3Se_7^{5-}$ (singlet, 1855 ppm). The corresponding ^{77}Se spectrum (−68 °C) confirmed the same three anions: $Tl_2Se_6^{6-}$ (triplet, 210 ppm and doublet, −103 ppm), $Tl_3Se_6^{5-}$ (doublet, 63 ppm and doublet of doublets, 31 ppm), and $Tl_3Se_7^{5-}$ (triplet, 274 ppm and doublet, 113 ppm) (Figure 4).

Determination of the Solution Structures of the $Tl_2Se_6^{6-}$, $Tl_3Se_6^{5-}$, and $Tl_3Se_7^{5-}$ Anions. The solution structures of the title anions were deduced by use of the spectral simulation program ISOTOPOMER[20] as described in a previous paper dealing with the solution characterizations of the related cubanoid $Tl_4Se_5^{4-}$ and $Tl_4Se_6^{4-}$ anions by $^{203,205}Tl$ and ^{77}Se NMR spectroscopy.[1] The spectral simulations for $Tl_2Se_6^{6-}$, $Tl_3Se_6^{5-}$, and $Tl_3Se_7^{5-}$ (Figures 2 and 3) are in excellent agreement with the experimental $^{203,205}Tl$ and ^{77}Se spectra and account for all of their features. Descriptions

(20) Santry, D. P.; Mercier, H. P. A.; Schrobilgen, G. J. *ISOTOPOMER, A Multi-NMR Simulation Program, version 3.02NTF*.; Snowbird Software, Inc.: Hamilton, ON, 2000.

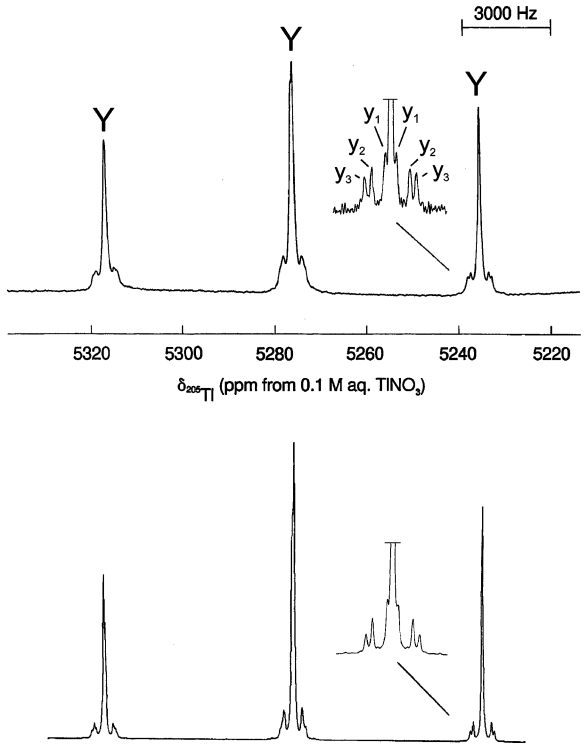

Figure 3. ^{205}Tl (liquid NH_3, −70 °C) NMR spectrum (115.444 MHz) of the Tl^I environment of the $Tl_3Se_6^{5-}$ anion obtained by extraction of $NaTl_{0.5}Se$ into liquid NH_3: experimental (upper trace) and calculated (lower trace) spectra. For clarity, only the subspectra associated with the central lines of the multiplets are labeled. Peak labels are assigned as follows: Y = T; $y_1 = T/^3d^{Tl^I}_{Se_t}$; $y_2 = T/^1d^{Tl^I}_{Se_{b''}}$; $y_3 = T/^1d^{Tl^I}_{Se_{b'''}}$. The multiplicity labels are defined in Table 5, footnote *c*.

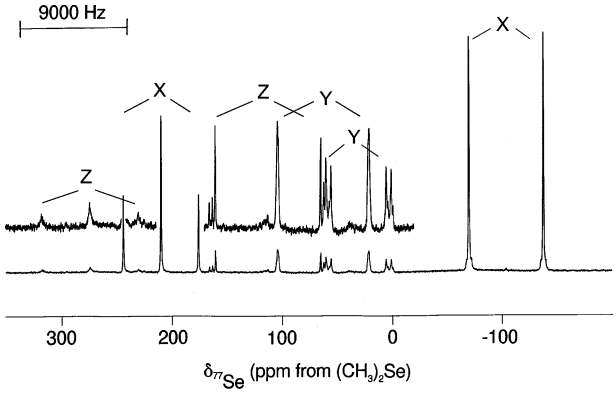

Figure 4. ^{77}Se (liquid NH_3, −68 °C) NMR spectrum (95.383 MHz) of the (X) $Tl_2Se_6^{6-}$, (Y) $Tl_3Se_6^{5-}$, and (Z) $Tl_3Se_7^{5-}$ anions obtained by extraction of $NaTl_{0.5}Se$ into liquid NH_3.

of the most important contributing isotopomers and their most prominent spectral features (indicated in Figures 2 and 3) are discussed below. Symbols used in the following discussion are defined in footnote c of Table 5 and are consistent with those used in ref 1.

(a) $Tl_2Se_6^{6-}$. The ^{205}Tl NMR spectrum of the $Tl_2Se_6^{6-}$ anion consists of a singlet in the Tl^{III} region flanked by doublet satellites. The Tl^{III} singlet (S) (1895 ppm, Figure 2) is assigned to the $^{205}Tl_2^{III}\ ^0Se_6$ isotopomeric subspectrum, and the associated satellite doublets arise from ^{203}Tl satellite subspectra ($S/^2d^{Tl^{III}}_{Tl_{III}}$) of the $^{205}Tl^{III}\ ^{203}Tl^{III}\ ^0Se_6$ isotopomer, which, in turn, arise from the intraenvironmental coupling, $^2J(^{205}Tl^{III}—^{203}Tl^{III})$ = 455 Hz (Table 5). The I_s/I_c ratios

Table 3. Chemical Shifts and Spin−Spin Coupling Constants for the $TlSe_3^{3-}$, $Tl_2Se_6^{6-}$, $Tl_3Se_6^{5-}$, and $Tl_3Se_7^{5-}$ Anions Obtained by the Extraction of NaTlSe[a]

	chemical shifts (ppm)		coupling constants, J (Hz)					
				$^{203,205}Tl-^{77}Se^{b,c}$				
anion	$^{205(203)}Tl$	^{77}Se	$^{205}Tl-^{203}Tl^{b}$	$Tl^{III}-Se$		$Tl^{I}-Se$	solvent/ligand	T (°C)[d]
Se^{2-}		-432					en/222	[0]
$TlSe_3^{3-}$	2875 (Tl^{III}), br	134, br		7413	[7190]		en/222	[0]
	2942 (Tl^{III}), br	78			[7208]		NH_3	−70 [−74]
$Tl_2Se_6^{6-}$	1877 s, vbr						en/THF/222	−15
	1886 (1885) (Tl^{III}), vbr			6120			NH_3	−30
	1891 (1890) (Tl^{III})	−106 (Se_t)	309 (326)	6312 (6256)	[6304]		NH_3	−50 [−52]
		212 (Se_b)		3237 (3125)	[3168]			
	1895 (1895) (Tl^{III})	−101 (Se_t)	412 (421)	6349 (6279)	[6343]		NH_3	−70 [−74]
		209 (Se_b)		3216 (3187)	[3210]			
	1897 (Tl^{III})		445	6365			NH_3	−76
				3220				
$Tl_3Se_6^{5-}$	1825 (1824) (Tl^{III}), br		3890 (3885)				en/222	0
	5300 (Tl^{I}), br		1321 (1385)					
	1849 (Tl^{III}), br		3979				en/THF/222	−15
			1428					
	1836 (1835) (Tl^{III}), br		4329 (4312)				NH_3	−30
			738 (736)					
	1836 (1835) (Tl^{III})		4517 (4480)	3178			NH_3	−50
			829 (835)					
	1836 (1835) (Tl^{III})	63 (Se_t)	4664 (4638)		[7782]		NH_3	−70 [−74]
	5284 (Tl^{I})	32 ($Se_{b''}$)	899 (909)	3153	[5127]	462 [453]		
	1836 (Tl^{III})		4721	3154		453	NH_3	−76
	5283 (Tl^{I})		923					
$Tl_3Se_7^{5-}$	1853 (1852) (Tl^{III})		801				NH_3	−50
	1857 (Tl^{III})		771				NH_3	−70
$Tl_4Se_6^{4-}$	∼5180 (Tl^{I}), vbr						en/222	0

[a] The symbols b″, b′, b, and t denote the bridging and terminal selenium environments as defined in structures I, II, and III. [b] Values in parentheses were obtained from the ^{203}Tl spectrum. [c] Values in square brackets were obtained from the ^{77}Se spectra. [d] Temperature in square brackets refers to the ^{77}Se spectra; otherwise the entry refers to both the ^{203}Tl and the ^{205}Tl spectra.

Table 4. Chemical Shifts and Spin−Spin Coupling Constants for the $Tl_2Se_6^{6-}$, $Tl_3Se_6^{5-}$, and $Tl_3Se_7^{5-}$ Anions Obtained by the Extraction of $NaTl_{0.5}Se$[a]

	chemical shift (ppm)		coupling constant, J (Hz)					
				$^{203,205}Tl-^{77}Se^{b,c}$				
anion	$^{205(203)}Tl$	^{77}Se	$^{205}Tl-^{203}Tl^{b}$	$Tl^{III}-Se$		$Tl^{I}-Se$	solvent	T (°C)
$Tl_2Se_6^{6-}$	1895 (1895) (Tl^{III})	−103 (Se_t)	455 (470)	6357 (6299) [6419] (Se_t)			NH_3	−70, −68
		210 (Se_b)		3221 (3192) [3248] (Se_b)				
$Tl_3Se_6^{5-}$	1833 (1832) (Tl^{III})	63 (Se_t)	4689 (4685)	7665 (7683) [7897] (Se_t)	124	(Se_t, ^3J)	NH_3	−70, −68
	5276 (Tl^{I})	31 ($Se_{b''}$)	918 (928)	5340 (5222) [5213] ($Se_{b''}$)	451	[443] ($Se_{b''}$)		
		n.o. ($Se_{b'''}$)		3145 (3146) ($Se_{b'''}$)	611	($Se_{b'''}$)		
		n.o. (Se_b)		∼1400 (Se_b)				
$Tl_3Se_7^{5-}$	1855 (1854) (Tl^{III})	113 (Se_t)	759 (754)	9266 (9247) [9125] (Se_t)			NH_3	−70, −68
		274 (Se_b)		4179 (4124) [4146] (Se_b)				
		n.o. ($Se_{b'}$)		∼2000 ($Se_{b'}$)				

[a] The symbols b‴, b″, b′, b, and t denote the bridging and terminal selenium environments as defined in structures I, II, and III. [b] Values in parentheses were obtained from the ^{203}Tl spectrum. [c] Values in square brackets were obtained from the ^{77}Se spectra.

indicate that each Tl^{III} nucleus is spin-coupled to one other Tl^{III} nucleus. Satellite doublet subspectra symmetrically disposed about each component of the singlet, $S/^1d^{Tl^{III}}_{Se_b}$ and $S/^1d^{Tl^{III}}_{Se_t}$, result from $^1J(^{205}Tl^{III}-^{77}Se_b) = 3221$ Hz and $^1J(^{205}Tl^{III}-^{77}Se_t) = 6357$ Hz of the isotopomers $^{205}Tl_2^{III}\ ^{77}Se_b\ ^0Se_5$ and $^{205}Tl_2^{III}\ ^{77}Se_t\ ^0Se_5$. The I_s/I_c ratios are consistent with two Se_b and two Se_t atoms bonded to each Tl atom (structure I).

The ^{77}Se NMR spectrum (Figure 4) of the $Tl_2Se_6^{6-}$ anion consists of two resonances in a ca. 1:2 intensity ratio, in agreement with the numbers of Se_t and Se_b atoms. The resonance at 210 ppm is a triplet [$^1J(^{77}Se_b-^{203,205}Tl^{III}) = 3248$ Hz] assigned to Se_b and the resonance at −103 ppm is a doublet [$^1J(^{77}Se_t-^{203,205}Tl^{III}) = 6419$ Hz] assigned to Se_t. Both resonances were assigned by comparison of the $^1J(^{77}Se-^{203,205}Tl^{III})$ couplings observed in the ^{77}Se spectrum with those observed in the $^{205(203)}Tl$ spectra.

The multiplet patterns and I_s/I_c ratios are consistent with a $Tl_2Se_6^{6-}$ anion containing two Tl^{III} atoms in which each Tl^{III} is bonded to two terminal (Se_t) and to two bridging (Se_b) selenium atoms. The Tl and bridging Se atoms form a Tl_2Se_2-ring with the Tl^{III} atom bonded to two unique exo-Se_t atoms (structure I).

(b) $Tl_3Se_6^{5-}$. The ^{205}Tl NMR spectrum of the $Tl_3Se_6^{5-}$ anion consists of a doublet and a triplet in the Tl^{III} and Tl^{I} regions, respectively. The most intense feature in the Tl^{III} region is a doublet (D) (1833 ppm; Figure 2) arising from a coupling between one Tl^{III} and one Tl^{I} nucleus of the isotopomers $^{205}Tl_2^{III}\ ^{205}Tl_y^{I}\ ^{203}Tl_{1-y}^{I}\ ^0Se_6$ ($y = 0-1$) (Table 6), where $^2J(^{205}Tl^{III}-^{205(203)}Tl^{I}) = 4689$ Hz. Each of

Table 5. The Most Abundant Natural Abundance Isotopomers and Subspectra Comprising the ^{205}Tl and ^{203}Tl NMR Spectra of the $Tl_2Se_6^{6-}$ Anion

$^{205}Tl_x^{III}\ ^{203}Tl_{2-x}^{III}$ $^{77}Se_z\ ^0Se_{6-z}^{6-}$ [a]			isotopomer fractional abundance[b]	multiplicity observed for the components of the subspectra in the Tl^{III} region[c]	
		^{77}Se		^{205}Tl	^{203}Tl
x	z	environments			
2	0		0.3097	S	−
1	0		0.2592	$S/^2d_{Tl^{III}}^{Tl^{III}}$	$S/^2d_{Tl^{III}}^{Tl^{III}}$
0	0		0.0542	−	S
2	1	(Se_t)	0.1016	$S/^1d_{Se_t}^{Tl^{III}}$	−
1	1	"	0.0425	$S/^2d_{Tl^{III}}^{Tl^{III}}/S/^1d_{Se_t}^{Tl^{III}}$	$S/^2d_{Tl^{III}}^{Tl^{III}}/^3d_{Se_t}^{Tl^{III}}$
1	1	"	0.0425	$S/^2d_{Tl^{III}}^{Tl^{III}}/S/^3d_{Se_t}^{Tl^{III}}$	$S/^2d_{Tl^{III}}^{Tl^{III}}/^1d_{Se_t}^{Tl^{III}}$
0	1	"	0.0178	−	$S/^1d_{Se_t}^{Tl^{III}}$
2	1	(Se_b)	0.0508	$S/^1d_{Se_b}^{Tl^{III}}$	−
1	1	"	0.0425	$S/^2d_{Tl^{III}}^{Tl^{III}}/^1d_{Se_b}^{Tl^{III}}$	$S/^2d_{Tl^{III}}^{Tl^{III}}/^1d_{Se_b}^{Tl^{III}}$
0	1	"	0.0089	−	$S/^1d_{Se_b}^{Tl^{III}}$
2	2	(Se_b,Se_t)	0.0167	$S/^1d_{Se_t}^{Tl^{III}}/^1d_{Se_b}^{Tl^{III}}$	−
1	2	"	0.0070	$S/^2d_{Tl^{III}}^{Tl^{III}}/^1d_{Se_t}^{Tl^{III}}/^1d_{Se_b}^{Tl^{III}}$	$S/^2d_{Tl^{III}}^{Tl^{III}}/^1d_{Se_b}^{Tl^{III}}/^3d_{Se_t}^{Tl^{III}}$
1	2	"	0.0070	$S/^2d_{Tl^{III}}^{Tl^{III}}/^1d_{Se_b}^{Tl^{III}}/^3d_{Se_t}^{Tl^{III}}$	$S/^2d_{Tl^{III}}^{Tl^{III}}/^1d_{Se_t}^{Tl^{III}}/^1d_{Se_b}^{Tl^{III}}$
0	2	"	0.0029	−	$S/^1d_{Se_t}^{Tl^{III}}/^1d_{Se_b}^{Tl^{III}}$
2	2	($2Se_t$)	0.0083	$S/^1d_{Se_t}^{Tl^{III}}/^3d_{Se_t}^{Tl^{III}}$	−
2	2	"	0.0042	$S/^1t_{Se_t}^{Tl^{III}}$	−
1	2	"	0.0070	$S/^2d_{Tl^{III}}^{Tl^{III}}/^1d_{Se_t}^{Tl^{III}}/^3d_{Se_t}^{Tl^{III}}$	$S/^2d_{Tl^{III}}^{Tl^{III}}/^1t_{Se_t}^{Tl^{III}}$
1	2	"	0.0017	$S/^2d_{Tl^{III}}^{Tl^{III}}/^1t_{Se_t}^{Tl^{III}}$	$S/^2d_{Tl^{III}}^{Tl^{III}}/^1d_{Se_t}^{Tl^{III}}/^3d_{Se_t}^{Tl^{III}}$
0	2	"	0.0015	−	$S/^1d_{Se_t}^{Tl^{III}}/^3d_{Se_t}^{Tl^{III}}$
0	2	"	0.0007	−	$S/^1t_{Se_t}^{Tl^{III}}$
2	2	($2Se_b$)	0.0021	$S/^1t_{Se_b}^{Tl^{III}}$	−
1	2	"	0.0017	$S/^2d_{Tl^{III}}^{Tl^{III}}/^1t_{Se_b}^{Tl^{III}}$	$S/^2d_{Tl^{III}}^{Tl^{III}}/^1t_{Se_b}^{Tl^{III}}$
0	2	"	0.0004	−	$S/^1t_{Se_b}^{Tl^{III}}$

[a] ^0Se denotes spinless selenium atoms. [b] Natural abundances of the spin-$^1/_2$ nuclides used to calculate isotopomer fractional abundances were taken from ref 21: ^{77}Se, 7.58%; ^{203}Tl, 29.5%; ^{205}Tl, 70.5%. Although all isotopomers were included in the simulations, only isotopomer fractional abundances ≥0.0001 are listed in the table. [c] S denotes a singlet. Lowercase letters d (doublet) and t (triplet) denote satellite couplings arising from $J(^{205}Tl-^{203}Tl)$ or $J(^{205(3)}Tl-^{77}Se)$. The left-hand superscript denotes the order of the J coupling; the right-hand superscript and subscript denote the two nuclei that are spin coupled. For example, in the ^{205}Tl spectrum, the description $S/^2d_{Tl^{III}}^{Tl^{III}}/^1d_{Se_b}^{Tl^{III}}$ denotes a SINGLET flanked by doublet satellites originating from $^2J(^{205}Tl^{III}-^{203}Tl^{III})$ and $^1J(^{205}Tl^{III}-^{77}Se_b)$. Each multiplicity description refers to a single set of selenium environments and its associated isotopomers.

the doublet components is flanked by doublet ^{203}Tl satellite subspectra ($D/^2d_{Tl_{III}}^{Tl^{III}}$) assigned to $^{205}Tl^{III}\ ^{203}Tl^{III}\ ^{205}Tl_y^{I}\ ^{203}Tl_{1-y}^{I}\ ^0Se_6$ ($y = 0-1$), which arise from the intraenvironmental coupling, $^2J(^{205}Tl^{III}-^{203}Tl^{III}) = 918$ Hz. The I_s/I_c ratios indicate that each Tl^{III} nucleus is spin-coupled to one Tl^{III} nucleus. Satellite doublet subspectra, $D/^1d_{Se_b}^{Tl^{III}}$, $D/^1d_{Se_{b''}}^{Tl^{III}}$, $D/^1d_{Se_{b'''}}^{Tl^{III}}$, and $D/^1d_{Se_t}^{Tl^{III}}$, symmetrically disposed about each component of the doublet were also observed and result from $^1J(^{205}Tl^{III}-^{77}Se_b) \sim 1400$ Hz, $^1J(^{205}Tl^{III}-^{77}Se_{b''}) = 5340$ Hz, $^1J(^{205}Tl^{III}-^{77}Se_{b'''}) = 3145$ Hz, and $^1J(^{205}Tl^{III}-^{77}Se_t) = 7665$ Hz of their respective isotopomers, $^{205}Tl_2^{III}\ ^{205}Tl_y^{I}\ ^{203}Tl_{1-y}^{I}\ ^{77}Se_b\ ^0Se_5$ ($D/^1d_{Se_b}^{Tl^{III}}$), $^{205}Tl_2^{III}\ ^{205}Tl_y^{I}$ $^{203}Tl_{1-y}^{I}\ ^{77}Se_{b''}\ ^0Se_5$ ($D/^1d_{Se_{b''}}^{Tl^{III}}$), $^{205}Tl_2^{III}\ ^{205}Tl_y^{I}\ ^{203}Tl_{1-y}^{I}$ $^{77}Se_{b'''}\ ^0Se_5$ ($D/^1d_{Se_{b'''}}^{Tl^{III}}$), and $^{205}Tl_2^{III}\ ^{205}Tl_y^{I}\ ^{203}Tl_{1-y}^{I}\ ^{77}Se_t\ ^0Se_5$ ($D/^1d_{Se_t}^{Tl^{III}}$) ($y = 0-1$). The I_s/I_c ratios are consistent with single selenium atoms in Se_b, $Se_{b''}$, $Se_{b'''}$, and Se_t environments (structure II). The $^2J(^{203}Tl^{III}-^{205(203)}Tl^{I}) = 4685$ Hz coupling associated with the $^{203}Tl_2^{III}\ ^{205}Tl_y^{I}\ ^{203}Tl_{1-y}^{I}\ ^0Se_6$ ($y = 0-1$) isotopomer was determined by recording the ^{203}Tl NMR spectrum (Figure 2b) and was confirmed by the $^2J(^{205}Tl-^{205(3)}Tl)/^2J(^{203}Tl-^{205(3)}Tl) = 1.001$ ratio ($\gamma(^{205}Tl)/\gamma(^{203}Tl) = 1.010$).[21]

The most intense feature in the Tl^{I} region of the ^{205}Tl spectrum is a triplet (T) (5276 ppm; Figure 3) arising from coupling between one Tl^{I} and two Tl^{III} atoms (vide supra), $^2J(^{205}Tl^{I}-^{205(203)}Tl^{III}) = 4689$ Hz, of the isotopomers $^{205}Tl_x^{III}\ ^{203}Tl_{2-x}^{III}\ ^{205}Tl_2^{I}\ ^0Se_6$ ($x = 0-2$). Satellite doublet subspectra, $T/^1d_{Se_{b''}}^{Tl^{I}}$, $T/^1d_{Se_{b'''}}^{Tl^{I}}$, and $T/^3d_{Se_t}^{Tl^{I}}$ symmetrically disposed about each component of the triplet, were also observed which result from $^1J(^{205}Tl^{I}-^{77}Se_{b''}) = 451$ Hz, $^1J(^{205}Tl^{I}-^{77}Se_{b'''}) = 611$ Hz, and $^3J(^{205}Tl^{I}-^{77}Se_t) = 124$ Hz of the respective isotopomers, $^{205}Tl_x^{III}\ ^{203}Tl_{2-x}^{III}\ ^{205}Tl_2^{I}\ ^{77}Se_{b''}\ ^0Se_5$ ($T/^1d_{Se_{b''}}^{Tl^{I}}$), $^{205}Tl_x^{III}\ ^{203}Tl_{2-x}^{III}\ ^{205}Tl_2^{I}\ ^{77}Se_{b'''}\ ^0Se_5$ ($T/^1d_{Se_{b'''}}^{Tl^{I}}$), and $^{205}Tl_x^{III}$ $^{203}Tl_{2-x}^{III}\ ^{205}Tl_2^{I}\ ^{77}Se_t\ ^0Se_5$ ($T/^3d_{Se_t}^{Tl^{I}}$; $x = 0-2$). The I_s/I_c ratios are consistent with one $Se_{b'''}$ and two $Se_{b''}$ atoms (structure II).

The $Tl_3Se_6^{5-}$ anion is a minor species in the ^{77}Se NMR spectrum (Figure 4) and is expected to give rise to four resonances in a 2(t):1(b):2(b″):1(b‴) ratio, in agreement with the relative numbers of Se_t, Se_b, $Se_{b''}$ and $Se_{b'''}$ atoms; however, the weaker resonances associated with Se_b and $Se_{b'''}$ were not observed. The Se_t resonance at 63 ppm is a doublet arising from $^1J(^{77}Se_t-^{205(203)}Tl^{III}) = 7897$ Hz. The resonance assigned to $Se_{b''}$ appears at 31 ppm and consists of a doublet-of-doublets arising from $^1J(^{77}Se_{b''}-^{205(203)}Tl^{III}) = 5213$ Hz (doublet) and $^1J(^{77}Se_{b''}-^{205(203)}Tl^{I}) = 443$ Hz (doublet). The resonances were assigned by comparison of the $J(^{77}Se-^{205(203)}Tl)$ couplings observed in the ^{77}Se spectrum with those observed in the $^{205,203}Tl$ spectra.

The ^{77}Se and $^{205,203}Tl$ multiplet patterns and I_s/I_c ratios are consistent with a $Tl_3Se_6^{5-}$ anion that contains two Tl^{III} atoms, each bonded to a single terminal (Se_t) and three bridging (Se_b, $Se_{b''}$, and $Se_{b'''}$) selenium atoms, and one Tl^{I} atom that is bonded to one $Se_{b'''}$ and two $Se_{b''}$ atoms. The Tl and bridging Se atoms form a *nido*-Tl_3Se_4 cage that is formally derived from the unknown cubanoid *closo*-$Tl_4Se_4^{4-}$ anion by removal of one Tl vertex and by bonding of the exo-Se_t atoms to two of the remaining Tl atoms (structure II). The additional splittings on the high-frequency transitions of the Tl(III) environment and on the low-frequency branch of the Tl(I) environment in the ^{205}Tl NMR spectrum of $Tl_3Se_6^{5-}$ arise from second-order splittings, which are also reproduced by the spectral simulation.

(c) $Tl_3Se_7^{5-}$. The ^{205}Tl NMR spectrum of the $Tl_3Se_7^{5-}$ anion in liquid NH_3 at −70 °C consists of a singlet (S) in the Tl^{III} region that results from $^{205}Tl_3^{III}\ ^0Se_7$ (Table 7). The

(21) Mason, J. In *Multinuclear NMR*; Mason, J., Ed.; Plenum Press: New York, 1987; Appendix, pp 623−629.

Table 6. The Most Abundant Natural Abundance Isotopomers and Subspectra Comprising the ^{205}Tl and ^{203}Tl NMR Spectra of the $Tl_3Se_6^{5-}$ Anion [For footnotes *a*−*c*, refer to Table 5. Capital letters D (doublet) and T (triplet) denote couplings arising from $J(^{205}Tl^{III}-^{203}Tl^{I})$ or $J(^{205}Tl^{III}-^{205}Tl^{I})$ which cannot be distinguished because of the small difference in absolute frequency between the ^{205}Tl and ^{203}Tl nuclides.]

$^{205}Tl_x^{III}\ ^{203}Tl_{2-x}^{III}\ ^{205}Tl_y^{I}\ ^{203}Tl_{1-y}^{I}\ ^{77}Se_z\ ^{0}Se_{5-z}^{3-}$ [a]					multiplicity observed for the components of the subspectra in the Tl^{III} region[c]		$^{205}Tl_x^{III}\ ^{203}Tl_{2-x}^{III}\ ^{205}Tl_y^{I}\ ^{203}Tl_{1-y}^{I}\ ^{77}Se_z\ ^{0}Se_{5-z}^{3-}$ [a]					multiplicity observed for the components of the subspectra in the Tl^{I} region[c]	
x	*y*	*z*	^{77}Se environments	isotopomer fractional abundance[b]	^{205}Tl	^{203}Tl	*x*	*y*	*z*	^{77}Se environments	isotopomer fractional abundance[b]	^{205}Tl	^{203}Tl
2	1	0		0.2184	D	−	2	1	0		0.2184	T	−
2	0	0		0.0914			1	1	0		0.1827		
							0	1	0		0.0382		
1	1	0		0.1827	$D/^{2}d_{Tl^{III}}^{Tl^{III}}$	$D/^{2}d_{Tl^{III}}^{Tl^{III}}$	2	0	0		0.0914	−	T
1	0	0		0.0765			1	0	0		0.0765		
0	1	0		0.0382	−	D							
0	0	0		0.0160									
2	1	1	Se_b	0.0179	$D/^{1}d_{Se_b}^{Tl^{III}}$	−	2	1	1	Se_b	0.0179	$T/^{3}d_{Se_b}^{Tl^{I}}$	−
2	0	1	"	0.0075			1	1	1	"	0.0150		
							0	1	1	"	0.0031		
1	1	1	Se_b	0.0150	$D/^{2}d_{Tl^{III}}^{Tl^{III}}/^{1}d_{Se_b}^{Tl^{III}}$	$D/^{2}d_{Tl^{III}}^{Tl^{III}}/^{1}d_{Se_b}^{Tl^{III}}$	2	0	1	Se_b	0.0075	−	$T/^{3}d_{Se_b}^{Tl^{I}}$
1	0	1	"	0.0063			1	0	1	"	0.0063		
							0	0	1	"	0.0013		
0	1	1	Se_b	0.0031	−	$D/^{1}d_{Se_b}^{Tl^{III}}$							
0	0	1	"	0.0013									
2	1	1	$Se_{b'''}$	0.0179	$D/^{1}d_{Se_{b'''}}^{Tl^{III}}$	−	2	1	1	$Se_{b'''}$	0.0179	$D/^{3}d_{Se_{b'''}}^{Tl^{I}}$	−
2	0	1	"	0.0075			1	1	1	"	0.0150		
							0	1	1	"	0.0031		
1	1	1	$Se_{b'''}$	0.0150	$D/^{2}d_{Tl^{III}}^{Tl^{III}}/^{1}d_{Se_{b'''}}^{Tl^{III}}$	$D/^{2}d_{Tl^{III}}^{Tl^{III}}/^{1}d_{Se_{b'''}}^{Tl^{III}}$	2	0	1	$Se_{b'''}$	0.0075	−	$T/^{3}d_{Se_{b'''}}^{Tl^{I}}$
1	0	1	"	0.0063			1	0	1	"	0.0063		
							0	0	1	"	0.0013		
0	1	1	$Se_{b'''}$	0.0031	−	$D/^{1}d_{Se_{b'''}}^{Tl^{III}}$							
0	0	1	"	0.0013									
2	1	1	$Se_{b''}$	0.0358	$D/^{1}d_{Se_{b''}}^{Tl^{III}}$	−	2	1	1	$Se_{''}$	0.0358	$T/^{1}d_{Se_{b''}}^{Tl^{I}}$	−
2	0	1	"	0.0150			1	1	1	"	0.0300		
							0	1	1	"	0.0031		
1	1	1	$Se_{b''}$	0.0150	$D/^{2}d_{Tl^{III}}^{Tl^{III}}/^{1}d_{Se_{b''}}^{Tl^{III}}$	$D/^{2}d_{Tl^{III}}^{Tl^{III}}/^{1}d_{Se_{b''}}^{Tl^{III}}$	2	0	1	$Se_{b''}$	0.0150	−	$T/^{1}d_{Se_{b''}}^{Tl^{I}}$
1	0	1	"	0.0063			1	0	1	"	0.0126		
							0	0	1	"	0.0026		
1	1	1	$Se_{b''}$	0.0150	$D/^{2}d_{Tl^{III}}^{Tl^{III}}/^{3}d_{Se_{b''}}^{Tl^{III}}$	$D/^{2}d_{Tl^{III}}^{Tl^{III}}/^{3}d_{Se_{b''}}^{Tl^{III}}$							
1	0	1	"	0.0063									
0	1	1	$Se_{b''}$	0.0063		$D/^{1}d_{Se_{b''}}^{Tl^{III}}$							
0	0	1	"	0.0026	−								

singlet is flanked by a ^{203}Tl satellite doublet subspectrum ($S/^{2}d_{Tl^{III}}^{Tl^{III}}$) assigned to $^{205}Tl_2^{III}\ ^{203}Tl^{III}\ ^{0}Se_7$, which arises from the intra-environmental coupling $^{2}J(^{205}Tl^{III}-^{203}Tl^{III}) = 759$ Hz. The third dominant feature is a triplet ($S/^{2}t_{Tl^{III}}^{Tl^{III}}$) in which the central transition overlaps with the main singlet arising from the $^{205}Tl^{III}\ ^{203}Tl_2^{III}\ ^{0}Se_7$ isotopomer. Weak, satellite doublet subspectra, $S/^{1}d_{Se_b}^{Tl^{III}}$, $S/^{1}d_{Se_{b'}}^{Tl^{III}}$, and $S/^{1}d_{Se_t}^{Tl^{III}}$, were observed, which were symmetrically disposed about the singlet as well as about each component of the triplet, corresponding to $^{1}J(^{205}Tl^{III}-^{77}Se_b) = 4179$ Hz, $^{1}J(^{205}Tl^{III}-^{77}Se_{b'}) \sim 2000$ Hz, and $^{1}J(^{205}Tl^{III}-^{77}Se_t) = 9266$ Hz. The I_s/I_c ratios are consistent with one Se_t and two Se_b atoms (structure III).

The ^{77}Se NMR spectrum (Figure 4) of the $Tl_3Se_7^{5-}$ anion, which is also a minor species, is expected to give rise to three resonances in an approximate 3:3:1 ratio, corresponding to Se_t, Se_b, and $Se_{b'}$. The least $Se_{b'}$ intense resonance of the $Tl_3Se_7^{5-}$ anion was not observed. The resonances at 274 and 113 ppm consist of a triplet [$^{1}J(^{77}Se_b-^{205(203)}Tl^{III}) = 4146$ Hz] and a doublet [$^{1}J(^{77}Se_t-^{205(203)}Tl^{III}) = 9125$ Hz], which are assigned to Se_b and Se_t, respectively, by comparison with the $J(^{77}Se-^{205(203)}Tl)$ couplings observed in the $^{205(203)}Tl$ spectra.

The multiplet patterns and I_s/I_c ratios are consistent with a $Tl_3Se_7^{5-}$ anion containing three Tl^{III} atoms in which each Tl^{III} atom is bonded to one terminal (Se_t), two bridging (Se_b) selenium atoms, and one bridging ($Se_{b'}$) selenium atom. The anion structure is also based on a *nido*-Tl_3Se_4 cage in which the Tl^{III} atom is bonded to an unique exo-Se_t atom (structure III).

Chemical Shifts and Coupling Constants. The $^{205/203}Tl$ chemical shifts for the $Tl_2Se_6^{6-}$, $Tl_3Se_6^{5-}$, and $Tl_3Se_7^{5-}$ anions exhibit the same trends as those of the related Tl^{III} ($TlCh_3^{3-}$),[2,3] Tl^{I} ($Tl_2Ch_2^{2-}$) (Ch = Se, Te),[2,3] and mixed Tl^{III}/Tl^{I} cubanoid anions ($Tl_4Se_5^{4-}$ and $Tl_4Se_6^{4-}$),[1] with the thallium resonances of the Tl^{III} anions being considerably more shielded than those of the Tl^{I} anions (Figure 5 and Table 4). Figure 5 also

Table 7. The Most Abundant Natural Abundance Isotopomers and Subspectra Comprising the ^{205}Tl and ^{203}Tl NMR Spectra of the $Tl_3Se_7^{5-}$ Anion [For footnotes *a*−*c*, refer to Table 5.]

$^{205}Tl_x^{III}\,^{203}Tl_{3-x}^{III}$ $^{77}Se_z\,^{0}Se_{7-z}^{5-}$ [a]				multiplicity observed for the components of the subspectra in the Tl^{III} region[c]	
x	*z*	^{77}Se environments	isotopomer fractional abundance[b]	^{205}Tl	^{203}Tl
3	0		0.2018	S	−
2	0		0.3209	$S/^2d^{Tl^{III}}_{Tl_{III}}$	$S/^2t^{Tl^{III}}_{Tl_{III}}$
1	0		0.1060	$S/^2t^{Tl^{III}}_{Tl_{III}}$	$S/^2d^{Tl^{III}}_{Tl_{III}}$
0	0		0.0148	−	S
3	1	$Se_{b'}$	0.0166	$S/^1d^{Tl^{III}}_{Se_{b'}}$	−
2	1	"	0.0208	$S/^2d^{Tl^{III}}_{Tl_{III}}/^1d^{Tl^{III}}_{Se_{b'}}$	$S/^2t^{Tl^{III}}_{Tl_{III}}/^1d^{Tl^{III}}_{Se_{b'}}$
1	1	"	0.0087	$S/^2t^{Tl^{III}}_{Tl_{III}}/^1d^{Tl^{III}}_{Se_{b'}}$	$S/^2d^{Tl^{III}}_{Tl_{III}}/^1d^{Tl^{III}}_{Se_{b'}}$
0	1	"	0.0012	−	$S/^1d^{Tl^{III}}_{Se_{b'}}$
3	1	Se_t	0.0497	$S/^1d^{Tl^{III}}_{Se_t}$	−
2	1	"	0.0416	$S/^2d^{Tl^{III}}_{Tl_{III}}/^1d^{Tl^{III}}_{Se_t}$	$S/^2d^{Tl^{III}}_{Tl_{III}}/^3d^{Tl^{III}}_{Se_t}$
1	1	"	0.0208	$S/^2d^{Tl^{III}}_{Tl_{III}}/^3d^{Tl^{III}}_{Se_t}$	$S/^2d^{Tl^{III}}_{Tl_{III}}/^1d^{Tl^{III}}_{Se_t}$
0	1	"	0.0036	−	$S/^1d^{Tl^{III}}_{Se_t}$
3	1	Se_b	0.0497	$S/^1d^{Tl^{III}}_{Se_b}$	−
2	1	"	0.0207	$S/^2d^{Tl^{III}}_{Tl_{III}}/^1d^{Tl^{III}}_{Se_b}$	$S/^2t^{Tl^{III}}_{Tl_{III}}/^3d^{Tl^{III}}_{Se_b}$
2	1	"	0.0415	$S/^2d^{Tl^{III}}_{Tl_{III}}/^1d^{Tl^{III}}_{Se_b}/^3d^{Tl^{III}}_{Se_b}$	$S/^2t^{Tl^{III}}_{Tl_{III}}/^1d^{Tl^{III}}_{Se_b}$
1	1	"	0.0086	$S/^2t^{Tl^{III}}_{Tl_{III}}/^3d^{Tl^{III}}_{Se_b}$	$S/^2d^{Tl^{III}}_{Tl_{III}}/^1d^{Tl^{III}}_{Se_b}$
1	1	"	0.0173	$S/^2t^{Tl^{III}}_{Tl_{III}}/^1d^{Tl^{III}}_{Se_b}$	$S/^2d^{Tl^{III}}_{Tl_{III}}/^1d^{Tl^{III}}_{Se_b}/^3d^{Tl^{III}}_{Se_b}$
0	1	"	0.0036	−	$S/^1d^{Tl^{III}}_{Se_b}$

clearly shows, for each oxidation state, that one can also differentiate between the coordination numbers of the Tl^{III} (4 or 3) and Tl^{I} (3 or 2) atoms, allowing unambiguous assignments of the local geometries of Tl^{III} and Tl^{I} (tetrahedral or trigonal planar) to be made. The Tl^{I} and Tl^{III} shieldings increase with increasing coordination number as observed for other main-group species.[22] In the present study, it is clear that Tl^{I} in $Tl_3Se_6^{5-}$, which is more shielded than Tl^{I} in $Tl_4Se_5^{4-}$ and $Tl_4Se_6^{4-}$, has a tetrahedral environment. The similarity of the Tl^{I} chemical shift of $Tl_3Se_6^{5-}$ to those of $Tl_4Se_5^{4-}$ and $Tl_4Se_6^{4-}$ is in accord with their related cubanoid geometries. The similar Tl^{III} chemical shifts of $Tl_2Se_6^{6-}$, $Tl_3Se_6^{5-}$, and $Tl_3Se_7^{5-}$ are consistent with structures having comparable tetrahedral environments. Thallium(III) in $Tl_4Se_5^{4-}$ is the most shielded Tl^{III} environment among the anion series. The increased shielding may be attributed to the three Tl^{I} atoms which withdraw less electron density from the Se_b atoms that also bridge the single Tl^{III} center.

As expected, the Se_t chemical shift in $Tl_3Se_6^{5-}$ (63 ppm) is similar to that in $Tl_3Se_7^{5-}$ (113 ppm) because the immediate, directly bonded environment of the Se_t atom(s) remains unchanged, i.e., one tetrahedral Tl^{III} atom and the same net anion charge. This correlation has also been noted for the Se_t chemical shifts of the $Tl_4Se_6^{4-}$ and $Tl_4Se_5^{4-}$ anions.[1] These terminal selenium chemical shifts are more deshielded than those of the $Tl_2^{III}Se_6^{6-}$ anion (−103 ppm), suggesting that more of the anion charge is localized on the terminal Se ligands in the case of $Tl_2^{III}Se_6^{6-}$.

The $^2J(Tl^{I}-Tl^{III})$ coupling for $Tl_3Se_6^{5-}$ (4689 Hz) is intermediate with respect to those of $Tl_4Se_5^{4-}$ (6272 Hz) and $Tl_4Se_6^{4-}$ (3682 Hz)[1] and is in accord with their similar geometries. Interestingly, the $^2J(Tl^{III}-Tl^{III})$ couplings in $Tl_2Se_6^{6-}$ (455 Hz), $Tl_3Se_7^{5-}$ (759 Hz), and $Tl_3Se_6^{5-}$ (918 Hz) are all considerably smaller than in $Tl_4Se_6^{4-}$ (1495 Hz).

In the case of $Tl_4Se_6^{4-}$, the trend $J(Tl^{I}-Tl^{III}) > J(Tl^{III}-Tl^{III})$ is observed,[1] and follows the valence s orbital populations on the coupled centers, in qualitative agreement with the formalism for the Fermi contact contribution to the *J*-coupling.[23,24] The Fermi contact term is proportional to the product of the s electron densities at the nuclei of the coupled centers and is expected to make a major, if not dominant, contribution to the coupling. As previously noted for the $Tl_4Se_5^{4-}$ and $Tl_4Se_6^{4-}$ anions, the Tl−Tl couplings vary only slightly with temperature and the nature of the solvent (Table 3).[1]

The $^1J(^{205}Tl-^{77}Se_t)$ couplings are larger than the $^1J(^{205}Tl-^{77}Se_{b,b',b'',b'''})$ couplings and are consistent with higher bond orders and shorter bond lengths for the $Tl^{III}-Se_t$ bond when compared with those of the $Tl^{I}-Se_{b'',b'''}$ and $Tl^{III}-Se_{b,b',b'',b'''}$ bonds.

Computational Results. There are a considerable number of group 13 analogues of the $Tl_2Se_6^{6-}$ anion, namely, $Al_2Se_6^{6-}$,[25,26] $Al_2Te_6^{6-}$,[27−29] $Ga_2S_6^{6-}$,[30−32] $Ga_2Se_6^{6-}$,[31−33] $Ga_2Te_6^{6-}$,[34] $In_2S_6^{6-}$,[35] $In_2Te_6^{6-}$,[36] and $Tl_2O_6^{6-}$.[37,38] Only one example other than the *nido*-cubanoid anion, $Tl_3Se_7^{5-}$, has been characterized, namely, *nido*-$In_3Te_7^{5-}$.[6]

(a) Geometry Optimizations. All optimized geometries for gas-phase anions are depicted in Figure 6, geometric parameters for $Tl_2Se_6^{6-}$, $[Tl_2Se_6^{6-}][4Na^+]$, $Tl_3Se_6^{5-}$, and $Tl_3Se_7^{5-}$ are listed in Table 8, and those for $Tl_4Se_8^{4-}$ are listed in Table 2 together with their experimental values. The calculated vibrational frequencies and their symmetries are given in Table S1.

(i) $Tl_2Se_6^{6-}$ and $[M_2Ch_6^{6-}][4Na^+]$ (M = Ga, In, Tl; Ch = S, Se, Te). Optimization using D_{2h} symmetry resulted in a stationary point with all vibrational frequencies real. Both Tl atoms are bonded to two terminal Se_t and two bridging Se_b atoms, with $Tl-Se_t$ and $Tl-Se_b$ bond lengths of 2.923 and 2.901 Å, respectively (Figure 6a). Although the gas-phase geometry of $Tl_2Se_6^{6-}$ was fully optimized at the MP2

(22) Mason, J. In *Multinuclear NMR*; Mason, J., Ed.; Plenum Press: New York, 1987; Chapter 3, pp 66−67.
(23) Jameson, J. In *Multinuclear NMR*; Mason, J., Ed.; Plenum Press: New York, 1987; Chapter 4, p 89.
(24) Pople, J. A.; Santry, D. P. *Mol. Phys.* **1964**, *8*, 1.
(25) Eisenmann, B.; Hofmann, A. *Z. Kristallogr.* **1991**, *197*, 141.
(26) Eisenmann, B.; Hofmann, A. *Z. Kristallogr.* **1991**, *197*, 173.
(27) Eisenmann, B.; Hofmann, A. *Z. Kristallogr.* **1991**, *197*, 139.
(28) Eisenmann, B.; Hofmann, A. *Z. Kristallogr.* **1991**, *197*, 157.
(29) Eisenmann, B.; Hofmann, A. *Z. Kristallogr.* **1991**, *197*, 253.
(30) Eisenmann, B.; Hofmann, A. *Z. Kristallogr.* **1991**, *197*, 143.
(31) Eisenmann, B.; Hofmann, A. *Z. Kristallogr.* **1991**, *197*, 147.
(32) Eisenmann, B.; Hofmann, A. *Z. Kristallogr.* **1991**, *197*, 155.
(33) Eisenmann, B.; Hofmann, A. *Z. Kristallogr.* **1991**, *197*, 153.
(34) Eisenmann, B.; Hofmann, A. *Z. Kristallogr.* **1991**, *197*, 145.
(35) Eisenmann, B.; Hofmann, A. *Z. Kristallogr.* **1991**, *197*, 151.
(36) Wang, C.; Haushalter, R. C. *Inorg. Chem.* **1997**, *36*, 3806.
(37) Hoppe, R.; Wagner, G.; Glaum, H. Z. *Anorg. Allg. Chem.* **1987**, *547*, 188.
(38) Wagner, G.; Hoppe, R. *Naturwissenschaften* **1987**, *74*, 97.

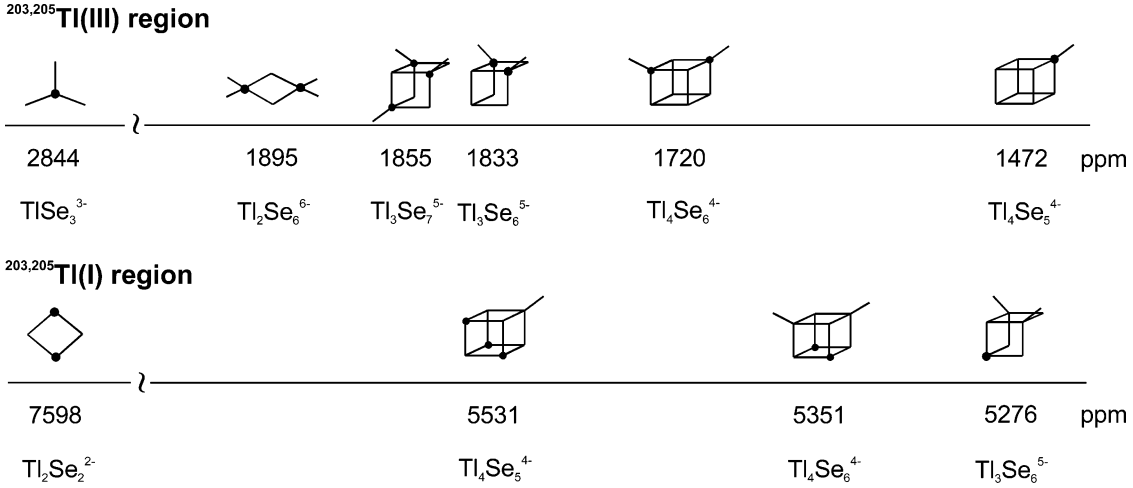

Figure 5. Shielding trends among Tl^{I} and Tl^{III} chemical shifts in the $TlSe_3^{3-}$, $Tl_2Se_2^{2-}$, $Tl_2Se_6^{6-}$, $Tl_3Se_6^{5-}$, $Tl_3Se_7^{5-}$, $Tl_4Se_5^{4-}$, and $Tl_4Se_6^{4-}$ anions.

level of theory to give a local minimum structure having D_{2h} symmetry, the bond length order $Tl-Se_t < Tl-Se_b$ implied from the $^1J(^{205/203}Tl-^{77}Se)$ couplings and observed in the crystal structures of the isovalent $M_2Ch_6^{6-}$ anions[6,30−35] was not reproduced. To investigate the effect of the anion environments in the solid state for the series of $M_2Ch_6^{6-}$ anions, the ion pairing was modeled using a simplified approach in which four Na^+ ions were placed on the C_2-symmetry axes of the anion close to the Se atoms, thus retaining the D_{2h} point symmetry for the ion-pair models $[M_2Ch_6^{6-}][4Na^+]$. This starting model is similar to, but of higher symmetry than the anion and cation arrangements in their crystal structures. Calculated and experimental (when available) bond lengths, bond angles, and energies for the fully MP2-optimized structures are given in Table S2. The ion-pair model, $[Tl_2Se_6^{6-}][4Na^+]$, is depicted in Figure 6b. Inspection of Table S2 reveals that the optimized ion-pair models consistently reproduce the experimental bond length order for the bond lengths over the entire anion series and provide geometries that are in good agreement with the solid-state structures of the alkali metal salts.

The stationary points for the simplified ion-pair models under D_{2h} symmetry have four imaginary low frequencies, as shown for $[Tl_2Se_6^{6-}][4Na^+]$ (Table S1). When the lowest imaginary frequencies are followed, two Na^+ ions move closer to the bridging Ch atoms, as shown in Figure S4 for $[M_2Ch_6^{6-}][4Na^+]$, but the $M_2Ch_6^{6-}$ skeletons do not change significantly. Thus, the geometry, though a transition state, gives a more realistic representation of the $Tl_2Se_6^{6-}$ anion in NH_3 solution than the structure of the gas-phase $Tl_2Se_6^{6-}$ anion at 0 K.

(ii) $Tl_4Se_8^{4-}$. Experimental and calculated MP2 bond parameters are given in Table 2. Optimization was started using the crystallographic coordinates. The experimental C_i structure is slightly twisted and its optimization at 0 K leads to the more symmetric D_{2h} structure (Figure 6c), which is a local minimum, with all frequencies real and 9.2 kcal mol^{-1} lower in energy than that calculated for the C_i anion symmetry in the crystal. All observed trends among bond lengths and bond angles are reproduced, e.g., $Tl_P-Se_t < Tl_P-Se_b < Tl_T-Se_{b'} < Tl_T-Se_b$.

(iii) $Tl_3Se_6^{5-}$ and $Tl_3Se_7^{5-}$. Optimization was started from the previously MP2-optimized C_{2v} structure of $Tl_4Se_6^{4-}$ [1] by removal of one Tl^+ cation from its *closo*-cubanoid structure. The optimization resulted in a *nido*-structure for $Tl_3Se_6^{5-}$ having C_s symmetry, which is a stationary point with all frequencies real (Figure 6d). For $Tl_3Se_7^{5-}$, a starting structure was derived from the $Tl_4Se_6^{4-}$ anion by exchanging one Tl^I for a Tl^{III} atom bonded to a terminal Se atom, thus forming a cubanoid *closo*-$Tl_4Se_7^{4-}$ anion from which, after optimization using C_{3v} symmetry, the Tl^I atom was removed. Final full optimization of *nido*-$Tl_3Se_7^{5-}$ under C_{3v} symmetry resulted in a local minimum with all frequencies real (Figure 6e).

(b) Natural Bond Orbital (NBO) Analyses. The NBO analyses were carried out for the optimized structures using the MP2 electron density. Natural charges, Mayer NAO valencies (total atomic bond orders),[39−41] overlap-weighted NAO bond orders, and a summary of natural Lewis structures are given in Table S3. Data for previously reported Tl/Se anions[1] are also provided for comparison. Details of the NBO analyses for the calculated species are given in Table S4. In each case, the bonding is well described by two center-two electron-bonded natural Lewis structures having less than 1% non-Lewis electrons (Table S3).

(i) $TlSe_3^{3-}$. The high natural charge (0.997) on Tl is in accord with the Tl^{III} oxidation state of $TlSe_3^{3-}$ (Figure 6f). The anion serves as a model for three-coordinate bonding to Tl^{III} with one π and three σ bonds. The π bond is comprised of four p orbitals, one from each atom of the anion, with the three Se p orbitals that are parallel to the three-fold axis of the anion, providing 96% of the electron occupancy (1.95 e) for the π orbital. The Se atoms contribute 77% of the NBO σ bond population (1.84 e). The NAO Tl−Se bond order (0.76) is higher than for a single bond (typically <0.6, see Table S3).

(39) Mayer, I. *Chem. Phys. Lett.* **1983**, *97*, 270.
(40) Mayer, I. *Theor. Chim. Acta* **1985**, *67*, 315.
(41) Mayer, I. *Int. J. Quantum Chem.* **1986**, *29*, 73.

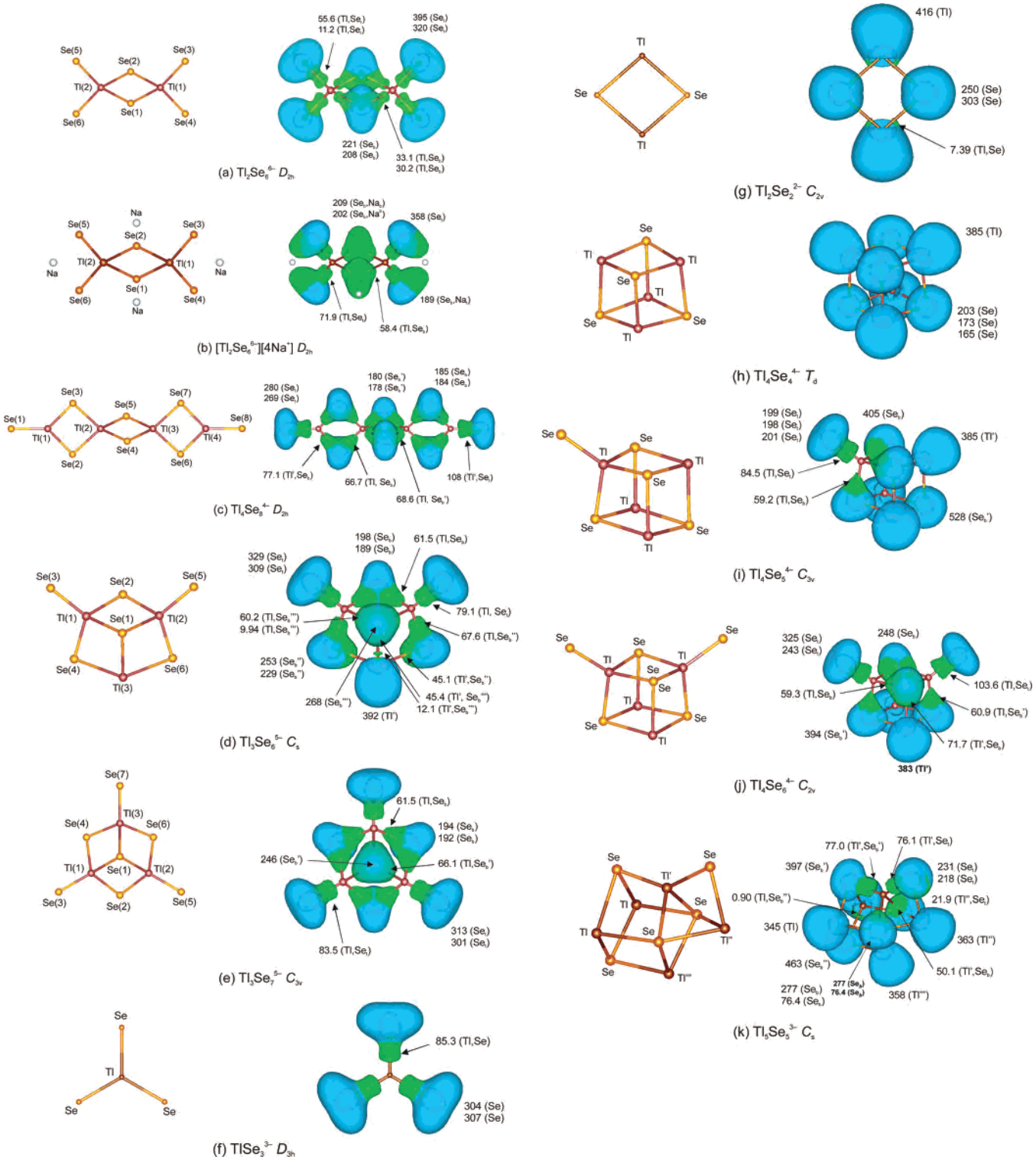

Figure 6. Calculated geometries at the MP2/Stutt RCL ECP (2d) level and electron localization function (ELF) lobes (HF level for MP2 geometries) for (a) $Tl_2Se_6^{6-}$, (b) $[Tl_2Se_6^{6-}][4Na^+]$, (c) $Tl_4Se_8^{4-}$, (d) $Tl_3Se_6^{5-}$, (e) $Tl_3Se_7^{5-}$, (f) $TlSe_3^{3-}$, (g) $Tl_2Se_2^{2-}$, (h) $Tl_4Se_4^{4-}$, (i) $Tl_4Se_5^{4-}$, (j) $Tl_4Se_6^{4-}$, and (k) $Tl_5Se_5^{3-}$. The symbol Tl denotes Tl^{III} and Tl′ denotes Tl^{I}. Monosynaptic (lone pair) ELF lobes are in blue and bisynaptic (bond pair) ELF lobes are in green.

(ii) $Tl_2Se_2^{2-}$. The thallium charge of 0.303 in this butterfly-shaped anion (Figure 6g) is much lower than in $TlSe_3^{3-}$ and a lone pair with a population of 1.95 e is assigned to the Tl atom. Much of this lone pair (92%) comes from the valence 6s orbital of Tl. This indicates that the 6s atomic orbital is almost fully occupied in accord with the Tl^{I} oxidation state. The NAO Tl−Se bond order (0.45) is normal for a single σ bond. It is interesting to note that the NBO analysis gives a bonding interaction between the Tl atoms (Tl···Tl, 2.890 Å) with a bond order (0.13) that is mainly of s character. This interaction, together with the repulsion between the lone pairs on each Tl and Se, gives rise to a butterfly-shaped, rather than to a planar, $Tl_2Se_2^{2-}$ anion. This bonding description is similar to that proposed in a previous study using LDFT and

Table 8. Calculated Geometries[a] for the $Tl_2Se_6^{6-}$ (D_{2h}), $[Tl_2Se_6^{6-}][4Na^+]$ (D_{2h}), $Tl_3Se_6^{5-}$ (C_s), $Tl_3Se_7^{5-}$ (C_{3v}), $TlSe_3^{3-}$ (D_{3h}), and $Tl_2Se_2^{2-}$ (D_{2h}) Anions

	$Tl_2Se_6^{6-}$	$[Tl_2Se_6^{6-}][4Na^+]$		$Tl_3Se_6^{5-}$	$Tl_3Se_7^{5-}$
		Bond Lengths (Å)			
Tl(1)−Se(1)	2.901	2.799	Tl(1)−Se(1)	2.916	2.910
Tl(1)−Se(2)	2.901	2.799	Tl(1)−Se(2)	2.801	2.770
Tl(1)−Se(3)	2.923	2.673	Tl(1)−Se(3)	2.756	2.698
Tl(1)−Se(4)	2.923	2.673	Tl(1)−Se(4)	2.769	2.770
Tl(2)−Se(1)	2.901	2.799	Tl(2)−Se(1)	2.916	2.910
Tl(2)−Se(2)	2.901	2.799	Tl(2)−Se(2)	2.801	2.770
Tl(2)−Se(5)	2.923	2.673	Tl(2)−Se(5)	2.756	2.698
Tl(2)−Se(6)	2.923	2.673	Tl(2)−Se(6)	2.769	2.770
			Tl(3)−Se(1)	3.031	2.910
			Tl(3)−Se(4)	3.078	2.770
			Tl(3)−Se(6)	3.078	2.770
			Tl(3)−Se(7)		2.698
Tl(1)...Tl(2)	4.291	4.292	Tl(1)...Tl(2)	4.053	3.934
			Tl(1)...Tl(3)	4.093	3.934
			Tl(2)...Tl(3)	4.093	3.934
		Bond Angles (deg)			
Se(1)−Tl(1)−Se(2)	84.6	79.9	Se(1)−Tl(1)−Se(2)	88.4	90.4
Se(1)−Tl(1)−Se(3)	117.4	116.0	Se(1)−Tl(1)−Se(3)	123.3	126.1
Se(1)−Tl(1)−Se(4)	117.4	116.0	Se(1)−Tl(1)−Se(4)	94.6	90.4
Se(1)−Tl(2)−Se(2)	84.6	79.9	Se(2)−Tl(1)−Se(3)	116.8	116.1
Se(1)−Tl(2)−Se(5)	117.4	116.0	Se(2)−Tl(1)−Se(4)	113.6	113.3
Se(1)−Tl(2)−Se(6)	117.4	116.0	Se(3)−Tl(1)−Se(4)	115.8	116.1
Se(2)−Tl(1)−Se(3)	117.4	116.0	Se(1)−Tl(2)−Se(2)	88.4	90.4
Se(2)−Tl(1)−Se(4)	117.4	116.0	Se(1)−Tl(2)−Se(5)	123.3	126.1
Se(2)−Tl(2)−Se(5)	117.4	116.0	Se(1)−Tl(2)−Se(6)	94.6	90.4
Se(2)−Tl(2)−Se(6)	117.4	116.0	Se(2)−Tl(2)−Se(5)	116.8	116.1
Se(3)−Tl(1)−Se(4)	102.9	110.3	Se(2)−Tl(2)−Se(6)	113.6	113.3
Se(5)−Tl(2)−Se(6)	102.9	110.3	Se(5)−Tl(2)−Se(6)	115.8	116.1
Tl(1)−Se(1)−Tl(2)	95.4	100.1	Se(1)−Tl(3)−Se(4)	86.3	90.4
Tl(1)−Se(2)−Tl(2)	95.4	100.1	Se(1)−Tl(3)−Se(6)	86.3	90.4
			Se(1)−Tl(3)−Se(7)		126.1
			Se(4)−Tl(3)−Se(6)	114.3	113.3
			Se(4)−Tl(3)−Se(7)		116.1
			Se(6)−Tl(3)−Se(7)		116.1
			Tl(1)−Se(1)−Tl(2)	88.0	85.0
			Tl(1)−Se(1)−Tl(3)	86.9	85.0
			Tl(2)−Se(1)−Tl(3)	86.9	85.0
			Tl(1)−Se(4)−Tl(3)	88.7	90.5
			Tl(1)−Se(2)−Tl(2)	92.7	90.5
			Tl(2)−Se(6)−Tl(3)	88.7	90.5

	$TlSe_3^{3-}$	$Tl_2Se_2^{2-}$
	Bond Lengths (Å)	
Tl−Se	2.673	2.890
	Bond Angles (deg)	
Se−Tl−Se	120	96.2
Tl−Se−Tl		81.3

[a] Geometries were calculated at the MP2 level using the Stutt RLC ECP (2d) basis sets.

NLDFT methods which gave a comparable Tl···Tl bond order (0.13−0.16).[2]

(iii) $Tl_2Se_6^{6-}$. Gas-Phase $Tl_2Se_6^{6-}$. The natural charge for the Tl^{III} atoms is 1.02, leaving each terminal Se atom with a charge of −1.47 and the bridging Se atoms with a charge of −1.09. The high valencies (2.25) of the Tl^{III} atoms are consistent with four single polar-covalent bonds having bond orders of 0.52 for the bridging Se atoms and 0.57 for the terminal Se atoms. There are small repulsive interactions among the Se atoms, with bond orders of −0.08 between the two bridging Se atoms, −0.08 between the pair of terminal Se atoms attached to the same Tl, and −0.04 for all the other Se−Se interactions. Although the Tl^{III} atoms are 4.291 Å apart, the interaction between them is slightly bonding, with a bond order of 0.07. All eight bonding orbitals have high electron populations, i.e., 1.82 (bridging bonds) and 1.79 (terminal bonds). The greatest contribution to bonding orbitals comes from the Se orbitals (82−87%).

Ion Pair Model, $[Tl_2Se_6^{6-}][4Na^+]$. The positive charges on the Tl^{III} atoms increase from 1.02 to 1.14, and the negative charges on the Se atoms decrease from −1.47 to −1.31 (terminal) and increase from −1.09 to −1.29 (bridging) when compared with the values for the isolated gas-phase anion. Thus, addition of positive ions renders the overall bonding of $Tl_2Se_6^{6-}$ slightly more ionic. The NBO natural charges on both "terminal" Na^+ ions (0.86) and "bridging" Na^+ ions (0.90) are significantly less than unit charges as a result of charge transfer from the terminal Se atoms to the Na^+ cations.

The valencies of Tl^{III} (2.51) are higher in this model than in the gas-phase anion (2.25). Four polar Tl−Se single bonds have bond orders of 0.47 for the bridging Se atoms and 0.73 for the terminal Se atoms. The interaction between Tl atoms,

now 4.292 Å apart, is decreased from a bond order of 0.07 to 0.03. Repulsive interactions between Se atoms are reduced to almost zero because of the presence of Na^+ ions. The NAO analysis of this ion-pair model also assigns significant bond orders between adjacent Na^+ ions and the bridging Se atoms (0.24) and between adjacent Na^+ ions and the terminal Se atoms (0.19), in accord with their reduced positive and negative charges.

The bonding orbitals of the anion in the ion-pair have higher electron populations (1.93, bridging bonds and 1.90, terminal bonds) when compared with the free gas-phase anion values (1.82 and 1.79, respectively). The Se contribution to bonding orbitals is less pronounced for the terminal bonds (76%), but remains at the same level (87%) for the bridging bonds in the ion pair. The addition of Na^+ ions draws electron density toward the terminal Se atoms increasing the bond order from 0.57 to 0.73, whereas the bridging bond order decreases from 0.52 to 0.47. Thus, the terminal bonds become more covalent while the bridging bonds become more polar.

(iv) $Tl_3Se_6^{5-}$. The natural charge for the two Tl^{III} atoms bonded to terminal Se atoms is 1.01, leaving each terminal Se atom with a charge of −1.38. The unique Tl^I atom does not have a terminal Se atom bonded to it and has a correspondingly lower natural charge (0.27), which is consistent with Tl^I. The $Se_{b''}$ atoms, which bridge the Tl^{III} and Tl^I atoms, both have charges of −1.21. The Se_b atoms bridging the two Tl^{III} atoms and the unique three-coordinate $Se_{b'''}$ atom each have charges of −1.05.

The high valencies of both Tl^{III} atoms (2.51) are consistent with four polar covalent bonds having bond orders of 0.57 and 0.60 to the bridging Se(2) and Se(4)/Se(6) atoms, respectively. The Tl^{III} atoms bonded to two terminal Se atoms possess bond orders of 0.71 and are the most covalent bonds in this anion. The Tl^I atom has a valency of 1.28, consistent with less bonding. The natural Lewis structure assigns one lone pair to the Tl^I atom, so that only three bonds are formed with Se(1) (bond order, 0.37) and with Se(4)/Se(6) (bond order, 0.36). The Se(1) atom, with three bonds, one to each Tl atom, has a higher valency (1.03) than the other Se atoms, i.e., 0.91 and 0.80 for bridging Se atoms having two bonds and 0.58 for terminal Se atoms having three valence electron lone pairs and one bond. The lower bond order (0.37) between the Se(1) and the Tl^I atom is reflected in its longer bond length (3.031 Å) when compared with the higher bond orders (0.45) and shorter bond lengths (2.916 Å) between the Se(1) and the Tl^{III} atoms.

(v) $Tl_3Se_7^{5-}$. The three Tl^{III} atoms of this anion have a natural charge of 1.01 and each terminal Se atom has a charge of −1.33. The three bridging Se atoms each have a charge of −1.03 and the unique $Se_{b'}$ bonded to all three Tl atoms has a natural charge of −0.95.

The high valency of each Tl^{III} (2.61) is consistent with three polar single bonds with bond orders of 0.59 to the bridging Se atoms and 0.75 to the terminal Se atoms. The Se(1) atom is equivalently bonded to all three Tl^{III} atoms, with bond orders of 0.46, and has a valency (1.09) that is higher than those of the bridging (0.95) and terminal (0.63) selenium atoms.

(vi) $Tl_4Se_8^{4-}$: Crystal Symmetry, C_i. The four Tl^{III} atoms gain most of their electron density from the bridging Se atoms, resulting in natural charges of 1.00. The terminal Se atoms have the most negative natural charges (−1.18) and the two central bridging Se atoms are less negative (−0.94).

The high valencies of the Tl^{III} atoms (2.81 for the central Tl atoms, 2.45 for the terminal Tl atoms) are consistent with four bonds to each Tl. Single bonds between the central Tl and the bridging Se atoms (bond order, 0.59−0.70) satisfy this bond count, but for the terminal Tl atoms, at least one formal double bond to a terminal Se atom (bond order, 0.92) is required to achieve the four bond count. The double bond is further supported by the high valencies (0.83) of the terminal Se atoms and by the high bond orders (0.92) between the terminal Se and Tl atoms. For this reason, a 16 BP−16 LP natural Lewis structure with terminal Tl−Se double bonds was also considered. The description of the formal bonding is only marginally different, with 0.74% of non-Lewis type electrons (compared to 0.67% of non-Lewis type electrons for the 14 BP−18 LP natural Lewis structure).

$Tl_4Se_8^{4-}$: Optimized D_{2h} Symmetry. The four Tl^{III} atoms have natural charges of 1.00. The terminal Se atoms have the most negative natural charge (−1.18), whereas the two central bridging Se atoms are the least negative (−0.92). All four of the remaining bridge Se atoms have charges of −0.95. Although the natural charges are the same as those in the crystal structure, the valencies on all atoms are lower. This indicates that the covalent bonding is overall stronger in the calculated C_i conformation (coordinates taken from the experimental crystal structure) than in the gas-phase optimized D_{2h} conformation.

The Tl^{III} atom valencies are lower (2.65 on the central Tl atoms and 2.36 on the terminal Tl atoms) than in the crystal structure, but are still consistent with four bonds to each Tl atom. The double bond is diminished and this is reflected in the slightly lower valencies (0.79) of the terminal Se atoms and by the lower bond orders (0.87) between the terminal Se and Tl, leading to less double bond character.

An alternative 16 BP−16 LP natural Lewis structure with terminal double bonds was also considered for this symmetry. The description of the formal bonding is only marginally better, with 0.76% electrons of the non-Lewis type (compared to 0.90% non-Lewis type electrons for 14 BP−18 LP Lewis structure). However, assignment of double bonds to the terminal $Tl'-Se_t$ bonds breaks the symmetry of the $Tl'-Se_b$ bridge bonds, which may explain why the symmetry is lowered from D_{2h} to C_i in the solid state.

(c) Electron Localization Function (ELF) Analyses. Electron localization function monosynaptic (lone-pair) and bisynaptic (bond-pair) lobes for $Tl_2Se_6^{6-}$, $[Tl_2Se_6^{6-}][4Na^+]$, $Tl_4Se_8^{4-}$, $Tl_3Se_6^{5-}$, and $Tl_3Se_7^{5-}$ are depicted in Figure 6. Details of the ELF analysis are given in Table S5. The previously described $TlSe_3^{3-}$,[2,3] $Tl_2Se_2^{2-}$,[2,3] $Tl_4Se_5^{4-}$,[1] $Tl_4Se_6^{4-}$,[1] $Tl_5Se_5^{3-}$,[1] and $Tl_4Se_4^{4-}$ [1] anions were also analyzed to provide

a more complete overview of the topologies of the electron pairs in these closely related systems and are also given in Figure 6.

No core basins are shown because Stuttgart pseudopotential basis sets were used. In all species studied, the Tl^{III} atoms are connected to Se atoms by V(Tl,Se) bond basins which are delocalized ($\lambda > 0.5$) in accord with the single-bonded NBO Lewis structures discussed above. For Tl^{I}, a monosynaptic V(Tl) basin having a population of 2.28−2.43 electrons and almost constant volume is shown to correspond to the occupied 6s orbital on Tl^{I}. Bridging selenium atoms show monosynaptic lone-pair basins V(Se) that overlap with the bond basins in accord with the σ NBO compositions where 80−90% of the electron population comes from Se (Table S3).

In $TlSe_3^{3-}$, there is no lone-pair basin, as expected for a Tl^{III} atom. Strong polar, but rather covalent Tl−Se bonding is shown as a bond basin with a rather large volume (85.3). On the other hand, a large lone-pair basin volume (416) on Tl^{I} in $Tl_2Se_2^{2-}$ and very small Tl−Se bonding basin (7.39) clearly illustrate the more ionic bonding characteristics of Tl^{I} when compared with Tl^{III}. Thus, ELF basin lobe presentations provide an easy way to confirm the oxidation states of Tl atoms in these Tl/Se anions, which are in agreement with the experiment.

The $Tl_2Se_6^{6-}$ and $[Tl_2Se_6^{6-}][4Na^+]$ ELF basin lobe shapes are very similar. The positive Na^+ cations, however, attract Se atom lone pairs so that they are drawn toward the cations. Although the population analysis tends to assign some bonding character to Se lone-pair basins, no separate bond basins are visible between Na^+ and the Se ligands.

For $Tl_4Se_8^{4-}$, the terminal V(Tl,Se_t) basins show somewhat larger volumes (101.8) and higher populations (1.63) than the singly bonded bridging basins (66.7−77.1 and 1.44−1.54), suggesting a stronger terminal bond. A structure with terminal double bonds was also shown to be a plausible bonding description in the NBO analysis of this anion (vide supra).

Conclusions

The new $Tl_2Se_6^{6-}$, $Tl_3Se_6^{5-}$, and $Tl_3Se_7^{5-}$ anions were unambiguously characterized in solution by ^{205}Tl, ^{203}Tl, and ^{77}Se NMR spectroscopy at their natural-abundance levels and their structures confirmed by full simulations and complete assignments of their isotopomeric ^{77}Se, ^{203}Tl, and ^{205}Tl subspectra. The $Tl_4Se_8^{4-}$ and $[Tl_2Se_4^{2-}]_\infty^1$ anions were isolated in the solid state as their [2,2,2-crypt-Na]$^+$ salts and structurally characterized by X-ray crystallography. The structures of the $Tl_3Se_6^{5-}$ and $Tl_3Se_7^{5-}$ anions are formally derived from the nido, cube-shaped Tl_3Se_4 cage and contain two and three exocyclic seleniums, respectively, bonded to Tl^{III} centers, while the $Tl_2Se_6^{6-}$, $Tl_4Se_8^{4-}$, and $Tl_2Se_4^{2-}$ anions are chains derived from Se-bridged Tl_2Se_2 rings. The geometries of the $Tl_2Se_6^{6-}$, $Tl_3Se_6^{5-}$, $Tl_3Se_7^{5-}$, and $Tl_4Se_8^{4-}$ anions have been shown to be energy minimized structures in which the bonding is well described in terms of two center-two electron bonds. Bonding analyses using NBO and ELF methods are complementary and show that Tl^{III}−Se bonds are more covalent than Tl^{I}−Se bonds. When Tl is in the +1 oxidation state, a lone pair assigned by NBO as an almost pure 6s valence orbital is clearly seen as a large spherical basin lobe in ELF representations, whereas the lone pair is absent for Tl^{III}. Thus, assignment of the formal +1 and +3 oxidation states of the Tl atoms in Tl/Se anions based on experimental findings can be readily confirmed by use of ELF or NBO calculations.

Experimental Section

Apparatus and Materials. All compounds employed were air sensitive; consequently, all manipulations were performed under rigorously anhydrous conditions and in the absence of oxygen on a glass vacuum line and in a two-station nitrogen-atmosphere drybox as previously described.[2]

Sodium metal (BDH Chemicals, 99.8%) was cleaned as previously described,[9] and freshly cut samples were only handled in a drybox. Thallium rods (Alfa Inorganics, 99%), selenium shot (Alfa Inorganics, 99.9%), and 2,2,2-crypt (1,10-diaza-4,7,13,16,21,24-hexaoxabicyclo[8.8.8]hexacosane; Merck, 99%) were dried in the evacuated port of a drybox for a minimum of 45 min followed by exposure to the atmosphere of the drybox for at least 2 days prior to use. The oxide layer on the thallium rod was shaved off with a scalpel inside a drybox prior to use. The ligand 18-crown-6 (1,4,7,10,13,16-hexaoxacyclooctadecane, Aldrich) was recrystallized twice from freshly distilled acetonitrile (Fisher Scientific Co.) and then vacuum distilled (<0.1 Torr) at 115 °C. The ligand was then transferred and stored inside a drybox.

All solvents were thoroughly dried, transferred by vacuum distillation, and stored in round-bottom flasks equipped with glass/Teflon stopcocks (J. Young). Ethylenediamine (Fisher Scientific Co., 99%), ethylamine (Aldrich, 99%), and tetrahydrofuran (Aldrich, 99.9%) were initially dried over CaH_2 powder (BDH Chemicals, 99.5%) and sodium (BDH Chemicals, 99.8%), respectively, for several weeks and then vacuum distilled onto, and stored over the same, but fresh, drying agent for at least an additional week prior to use. Anhydrous ammonia (Matheson, 99.99%) was condensed from a gas cylinder at −78 °C into a previously dried tube containing freshly cut sodium metal and was stored at −78 °C for at least one week prior to use. Dimethylformamide (BDH Chemicals, 99%) was dried over molecular sieves (3 Å, Fisher Scientific) which were activated by heating overnight under dynamic vacuum at ca. 250 °C.

Preparation of NaTlSe and $NaTl_{0.5}Se$. The NaTlSe and $NaTl_{0.5}Se$ alloys were prepared as previously described[2] by fusion of the elements in the required molar ratios inside a thick-walled Pyrex tube. The following amounts were used. NaTlSe: Na, 0.2470 g, 10.744 mmol; Tl, 2.1059 g, 10.304 mmol; Se, 0.8164 g, 10.339 mmol. $NaTl_{0.5}Se$: Na, 0.3146 g, 13.684 mmol; Tl, 1.3392 g, 6.553 mmol; Se, 1.0415 g, 13.190 mmol. The resulting alloys were ground into fine powders inside a drybox.

Preparation of the $Tl_2Se_6^{6-}$, $Tl_3Se_6^{5-}$, and $Tl_3Se_7^{5-}$ Solutions for NMR Spectroscopy. The anion solutions were prepared by extracting NaTlSe in en or en/THF in the presence of an excess of 2,2,2-crypt with respect to Na^+ and by extracting NaTlSe and $NaTl_{0.5}Se$ in the absence of 2,2,2-crypt in liquid NH_3. The resulting red−orange (NaTlSe) and deep red ($NaTl_{0.5}Se$) solutions were isolated for NMR spectroscopy as previously described. The following quantities of reagents were used to prepare the alloy extracts: for extraction in en or en/THF, NaTlSe: 0.1495 g, 0.488

mmol; 2,2,2-crypt: 0.2004 g, 0.532 mmol; for extraction in NH_3, NaTlSe [$NaTl_{0.5}Se$]: 0.5514 [0.3594] g, 1.800 [1.757] mmol.

NMR Spectroscopy. The ^{203}Tl and ^{205}Tl NMR spectra were recorded on a Bruker AC-200 (4.698 T) pulse spectrometer by inserting a 10-mm Bruker AC-300 broad-band probe (13.968−121.497 MHz) into an AC-200 (4.698 T) cryomagnet. The ^{77}Se NMR spectra were recorded on a Bruker AC-200 (4.698 T) (NaTlSe: 0 °C, en) and the AM-500 (11.744 T) (NaTlSe: −52 and −74 °C, NH_3; $NaTl_{0.5}Se$: −68 °C, NH_3) pulse spectrometers. Spectra were routinely obtained without locking (field drift < 0.1 Hz hr^{-1}) using 10-mm probes broad banded over the frequency ranges 9−81 (4.698 T) and 23−202 (11.744 T) MHz. The observed spectrometer frequencies were 95.383 (^{77}Se), 114.320 (^{203}Tl), and 115.447 (^{205}Tl) MHz (4.698 T), and 95.383 MHz (^{77}Se) (11.744 T). Free-induction decays were typically accumulated in 16 or 32 K memories. Spectral width settings of 25−100 kHz were employed, yielding resolutions of 3.05−6.10 Hz/data point and acquisition times of 0.328−0.164 s, respectively. A relaxation delay of 1.00 s was applied in the case of ^{77}Se. Typically, 10 000−100 000 transients were accumulated depending on the concentrations and sensitivities of the nuclides under study. Pulse-width settings corresponding to a bulk magnetization tip angle of ∼90° were 10.0 (^{205}Tl), 10.0 (^{77}Se, 11.744 T), and 20.0 (^{203}Tl) μs. Line broadening parameters used in the exponential multiplication of the free induction decays were 10−20 Hz for narrow lines and 100 Hz for broad lines. To enhance the resolution of some satellite peaks in the ^{205}Tl and ^{203}Tl NMR spectra and determine the *J*-couplings, the corresponding free-induction decays were transformed with the use of Gaussian line shapes rather than the conventional Lorentzian line shapes. For the Gaussian line shapes, broadening factors between 0.1 and 0.5 and the negative of the line-broadening parameters used for Lorentzian line shapes were employed. Variable-temperature spectra were recorded using the variable-temperature controllers of the spectrometers, and temperatures (accurate to ±1.0 °C and stable to within ±0.10 °C) were checked by placing a copper−constantan thermocouple into the sample region of the probe. Samples were allowed to equilibrate for at least 5 min while spinning before spectral accumulations were begun.

The ^{77}Se, ^{203}Tl, and ^{205}Tl chemical shifts were referenced externally to neat samples of $(CH_3)_2Se$ and 0.1 M aqueous $TlNO_3$ at 24 °C. According to the chemical shift convention used, a positive (negative) shift signified a chemical shift to high (low) frequency of the reference sample.

Simulation of NMR Spectra. The ^{203}Tl and ^{205}Tl NMR spectra of the $Tl_2Se_6^{6-}$, $Tl_3Se_6^{5-}$, and $Tl_3Se_7^{5-}$ anions were simulated as described previously using the computer program ISOTOPOMER.[20]

Crystal Growth of [2,2,2-crypt-Na]$_4$[Tl$_4$Se$_8$]·en and [2,2,2-crypt-Na]$_2$[Tl$_2$Se$_4$]·en. Extraction of $NaTl_{0.5}Se$ (0.0540 g, 0.264 mmol) in en in the presence of an equimolar mixture of 18-crown-6 (0.0388 g, 0.147 mmol) and 2,2,2-crypt (0.0524 g, 0.139 mmol) with respect to Na^+ gave rise to a deep red−orange solution. Vapor diffusion of THF into the en extract (1:3 v/v) over a period of several days resulted in the formation of orange plates of [2,2,2-crypt-Na]$_2[Tl_2Se_4]^1_\infty$·en ($0.10 \times 0.15 \times 0.22$ mm^3) and orange cubes of [2,2,2-crypt-Na]$_4$[Tl_4Se_8]·en ($0.05 \times 0.05 \times 0.05$ mm^3).

Crystal Isolation and Mounting. The crystals degraded rapidly under dynamic vacuum, indicating that solvent loss from the crystal lattices had occurred, and consequently, were subsequently manipulated inside a glovebag, located near the imaging plate of the diffractometer, which had been previously flushed for three days with dry argon and then filled with argon.

A bulk crystalline sample was recovered inside the glovebag and was deposited in a Petri dish containing perfluorodecaline. The Petri dish was then removed from the glovebag and was placed under a stereo-zoom microscope located less than 60 cm away from the diffractometer. Suitable single crystals were selected from the perfluorodecaline by using glass fibers which were coated at one end with Apiezon H grease (Apiezon Products, Manchester, England) and which had already been attached at the other end to the goniometer head of the diffractometer. Once the crystals were attached to the glass fibers, they were immediately mounted on the diffractometer within a stream of cold nitrogen gas at −100 °C.

Collection and Reduction of X-ray Data. Crystal data were collected on a Stoe imaging plate diffractometer system equipped with a single-circle goniometer and a graphite monochromator. Molybdenum radiation ($\lambda = 0.71073$ Å) was used.

Solution and Refinement of the Structures. All calculations were performed using the SHELXTL-Plus package[42] for structure determination, refinement, and molecular graphics. The XPREP program[42] was used to confirm the unit-cell dimensions and the crystal lattices. A solution was obtained by using conventional direct methods which located the general and/or special positions of the main-group and alkali-metal atoms. The full-matrix least-squares refinement of the positions and isotropic thermal parameters of the assigned atoms located the general and/or special positions of the C, N, and O atoms of the 2,2,2-crypt-Na^+ cations. Ethylenediamine solvent molecules were assigned after the atoms of the anions and cations were refined with anisotropic displacement parameters and any disorder was satisfactorily modeled. The occupancy for the disordered solvent molecules was refined (60:40). Crystallographically well-behaved and disordered solvent molecules could also be refined with anisotropic thermal parameters. Hydrogen-atom positions were calculated (d(C−H) = 0.96 Å, d(O−H) = 0.82 Å, d(N−H) = 0.96 Å), and U(H) was fixed to $-1.2 \times U$(C), U(O), or U(N). During the final stages of the refinement, all reflections with $F^2 < -2\sigma(F^2)$ were suppressed and weighting factors recommended by the refinement program were introduced. The maximum electron densities in the final difference maps were located around the anions.

Calculations. The ab initio molecular orbital calculations were performed at the Møller−Plesset perturbation correction for electron correlation to the second-order (MP2) level of theory as implemented in the Gaussian 98 program.[43] Stuttgart semi-relativistic large core and effective core pseudopotential basis sets of the Gaussian 98 package (SDDAll keyword) augmented with two d-type polarization functions by Huzinaga[44] were used for all calculated species. The geometries were fully optimized at the MP2

(42) Sheldrick, G. M. *SHELXTL-Plus, release 4.21/V.*; Siemens Analytical X-ray Instruments Inc.: Madison, WI, 1993.

(43) Frisch, M. J.; Trucks, G. W.; Schlegel, H. B.; Scuseria, G. E.; Robb, M. A.; Cheeseman, J. R.; Zakrzewski, V. G.; Montgomery, J. A., Jr.; Stratmann, R. E.; Burant, J. C.; Dapprich, S.; Millam, J. M.; Daniels, A. D.; Kudin, K. N.; Strain, M. C.; Farkas, O.; Tomasi, J.; Barone, V.; Cossi, M.; Cammi, R.; Mennucci, B.; Pomelli, C.; Adamo, C.; Clifford, S.; Ochterski, J.; Petersson, G. A.; Ayala, P. Y.; Cui, Q.; Morokuma, K.; Salvador, P.; Dannenberg, J. J.; Malick, D. K.; Rabuck, A. D.; Raghavachari, K.; Foresman, J. B.; Cioslowski, J.; Ortiz, J. V.; Baboul, A. G.; Stefanov, B. B.; Liu, G.; Liashenko, A.; Piskorz, P.; Komaromi, I.; Gomperts, R.; Martin, R. L.; Fox, D. J.; Keith, T.; Al-Laham, M. A.; Peng, C. Y.; Nanayakkara, A.; Challacombe, M.; Gill, P. M. W.; Johnson, B.; Chen, W.; Wong, M. W.; Andres, J. L.; Gonzalez, C.; Head-Gordon, M.; Replogle, E. S.; Pople, J. A.; *Gaussian 98*, revision A.7; Gaussian, Inc.: Pittsburgh, PA, 1998.

(44) Huzinaga, S.; Andzelm, J.; Klobukowski, M.; Radzio-Andzelm, E.; Sakai, Y.; Tatewaki, H. *Gaussian Basis Sets for Molecular Calculations*; Physical Science Data 16; Elsevier: Amsterdam, 1984.

level using analytical gradient methods. The natural bond orbital (NBO) analysis was conducted using the program NBO, version 3.1,[45] as implemented in the Gaussian 98 program package.[43] The Silvi−Savin[46,47] approach to chemical bonding, which is based on a topological analysis of the gradient field of the electron localization function (ELF) of Becke and Edgecombe,[48] was carried out using the TopMod program package.[49] Further details of ELF analysis have been given earlier.[50,51]

Acknowledgment. We thank the Natural Sciences and Engineering Research Council (NSERC) of Canada for their support in the form of a research grant. We also thank the Ontario Ministry of Education and Training for the award of a graduate scholarship to A.M.P. We gratefully acknowledge Prof. Arndt Simon, Max-Planck-Institut, Stuttgart, for making the Stoe imaging plate diffractometer system available. The use of computer facilities at the Finnish IT Center for Science is also gratefully acknowledged.

Supporting Information Available: Packing of [2,2,2-crypt-Na]$_2$[Tl_2Se_4]$^1_\infty$·en along the *b*-axis (Figure S1), ^{205}Tl and ^{203}Tl NMR spectra (0 °C) of the solution obtained by extraction of NaTlSe in en/2,2,2-crypt (Figure S2), ^{205}Tl and ^{203}Tl NMR spectra (−15 °C) of the solution obtained by extraction of NaTlSe in en/THF/2,2,2-crypt (Figure S3), imaginary frequencies for the [$M_2Ch_6^{6-}$][$4Na^+$] ion pairs (Figure S4), calculated fundamental vibrational frequencies (cm^{-1}) and assignments (Table S1), bonding and lone-pair NBOs (Table S2), ELF parameters (Table S3), MP2-optimized energies (Table S4), and an X-ray crystallographic file in CIF format for the structure determination [2,2,2-crypt-Na]$_4$[Tl_4Se_8]·en and [2,2,2-crypt-Na]$_2$[Tl_2Se_4]$^1_\infty$·en. This material is available free of charge via the Internet at http://pubs.acs.org.

IC0510922

(45) Glendening, E. D.; Reed, A. E.; Carpenter, J. E.; Weinhold, F. *NBO*, version 3.1; Gaussian, Inc.; Pittsburgh, PA, 1990.
(46) Silvi, B.; Savin, A. *Nature* **1994**, *371*, 683.
(47) Savin, A.; Silvi, B.; Colonna, F. *Can. J. Chem.* **1996**, *74*, 1088.
(48) Becke, A. D.; Edgecombe, K. E. *J. Chem. Phys.* **1990**, *92*, 5397.
(49) Noury, S.; Krokidis, X.; Fuster, F.; Silvi, B.; University of Paris VI: Paris, 1998.
(50) Mercier, H. P. A.; Moran, M. D.; Sanders, J. C. P.; Schrobilgen, G. J.; Suontamo, R. J. *Inorg. Chem.* **2005**, *44*, 49.
(51) Mercier, H. P. A.; Moran, M. D.; Schrobilgen, G. J.; Suontamo, R. J. *J. Fluorine Chem.* **2004**, *125*, 1563.